Proposal for the J-PARC 30-GeV Proton Synchrotron

Pion-induced phi-meson production on the proton

Takatsugu Ishikawa[a] and Hiroaki Ohnishi

Research Center for Electron Photon Science (ELPH),

Tohoku University, Sendai, Miyagi 982-0826, Japan

Kazuya Aoki, Ryotaro Honda, Yuhei Morino,

Kyoichiro Ozawa, Shin'ya Sawada, and Hitoshi Takahashi

Institute of Particle and Nuclear Studies (IPNS),

High Energy Accelerator Research Organization (KEK), Tsukuba, Ibaraki 305-0801, Japan

Wen-Chen Chang

Institute of Physics, Academia Sinica, Taipei 11529, Taiwan

Atsushi Hosaka, Tomoaki Hotta, Hiroyuki Noumi, Kotaro Shirotori, and Yorihito Sugaya

Research Center for Nuclear Physics (RCNP),

Osaka University, Ibaraki, Osaka 567-0047, Japan

Yudai Ichikawa, Hiroyuki Sako, and Kiyoshi Tanida

Advanced Science Research Center (ASRC),

Japan Atomic Energy Agency (JAEA), Tokai, Ibaraki 319-1195, Japan

Motoi Inaba

Faculty of Industrial Technology, Tsukuba University

of Technology, Tsukuba, Ibaraki 305-8520, Japan

Masashi Kaneta

Department of Physics, Graduate School of Science,

Tohoku University, Sendai, Miyagi 980-8578, Japan

Sang-Ho Kim

Department of Physics and Origin of Matter and Evolution of Galaxy (OMEG) Institute,

Soongsil University, Seoul 06978, Republic of Korea

Keigo Mizutani and Lubomir Pentchev

Thomas Jefferson National Accelerator Facility, Newport News, VA 23606, USA

Megumi Naruki

Department of Physics, Graduate School of Science,

Kyoto University, Kyoto, Kyoto 606-8502, Japan

Igor I Strakovsky

Institute for Nuclear Studies and Physics Department,

The George Washington University, Washington, DC 20052, USA

Tomonori Takahashi and Satoshi Yokkaichi

Nishina Center for Accelerator-Based Science,

Institute of Physical and Chemical Research (RIKEN), Wako, Saitama 351-0198, Japan

Natsuki Tomida

Center for Science Adventure and Collaborative Research Advancement (SACRA),

Graduate School of Science, Kyoto University, Kyoto, Kyoto 606-8502, Japan

PACS numbers: 13.60.Le, 14.20.Gk, 13.75.Gx

[a] Spokesperson: ishikawa@lns.tohoku.ac.jp

EXECUTIVE SUMMARY

reaction:	$\pi^- p \to \phi n$
beamline:	high-intensity high-momentum secondary beamline
beam:	negative pions (π^-s) with an intensity corresponding to the 400-W loss
	(2-s spill, 5.2-s cycle; unseparated negatively charged particles)
target:	liquid hydrogen with a thickness of 200 mm
detector:	the modified E16 spectrometer
beamtime:	5 days for detector commissioning
	10 days for 1.6 GeV/c
	10 days for 1.8 GeV/c
	10 days for 2.0 GeV/c
	10 days for 2.2 GeV/c
	10 days for 2.4 GeV/c

We measure the cross sections for the $\pi^- p \to \phi n$ reaction to study the nucleon resonances coupling to the ϕ meson and nucleon, which are expected to appear in the s-channel intermediate state of the reaction. We use several incident negative-pion (π^-) momenta from 1.6 to 2.4 GeV/c and the modified E16 spectrometer with large acceptance for detecting K^+K^- pairs from the ϕ decays. We assume the thickness of the liquid hydrogen target is 200 mm. The high-intensity high-momentum secondary beamline is expected to be constructed step by step. We require the beam intensity of π^-s corresponding to the 400-W loss of the primary beam at the Lambertson magnet. The proposed experiment can be performed at an early stage of the beamline construction.

CONTENTS

Executive Summary 3

Abstract 5

I. Introduction 7

A. Unidentified bump at $W = 2.2$ GeV in $\gamma p \to \phi p$ 8

B. Non observation of the P_c pentaquark baryons in $\gamma p \to J/\psi p$ 12

C. Different ϕN scattering lengths obtained from different methods 13

II. $\pi^- p \to \phi n$ reaction 14

A. Existing data 15

B. Expected cross sections 18

C. Kinematics 22

III. Experiment 25

A. Negative-pion beam 25

B. Modified E16 spectrometer 27

C. Acceptance for detecting K^+K^- pairs 30

D. Yield estimation 32

IV. Summary 34

A. Exchange particle in $\pi^- p \to \phi n$ at high incident momenta 34

B. Spin density matrix of ϕ in $\pi^- p \to \phi n$ 35

C. Study of P_c baryons via $\pi^- p \to J/\psi n$ 38

D. Study of ϕN interaction via the near-threshold $\pi^- p \to \phi n$ reaction 39

References 41

ABSTRACT

There exist several puzzles in the ϕN and $J/\psi N$ systems, which we call the vector-meson and nucleon (VN) puzzles, and major three issues are as follows:

1. ϕ photoproduction on the proton shows an unidentified bump at the center-of-mass energy $W = 2.2$ GeV in $d\sigma/dt|_{t=-|t|_{\rm min}}$ as a function of W,

2. J/ψ photoproduction on the proton does not show any peaks corresponding to the P_c pentaquark baryons observed in the $J/\psi p$ invariant-mass spectra, and

3. ϕ photoproduction experiments provide completely different scattering lengths from those determined in other methods.

Photoproduction of ϕ (J/ψ) mesons dominantly takes place in the t-channel exchange of multi-gluons. Here, incident photons are converted into certain vector mesons, and elastic scattering occurs on the nucleon. The angular distribution of the produced vector mesons shows forward peaking even at incident energies close to the production threshold. It is difficult to obtain information on s-channel ϕN ($J/\psi N$) intermediate states. In other words, a ϕN ($J/\psi N$) resonance state is difficult to be identified in a photoproduction experiment owing to the vector-meson properties of the photon. Suppression of the s-channel contribution also makes it difficult to extract the S-wave ϕN component for determining the ϕN scattering length.

Pion-induced ϕ (J/ψ) production on the proton, $\pi^- p \to \phi n$ ($\pi^- p \to J/\psi n$), is definitely a missing piece to understand the ϕN ($J/\psi N$) system. It should be noted that currently no N^*s coupling to ϕN are listed in the Review of Particle Physics. It enhances the s-channel ϕN ($J/\psi N$) contribution as compared with photoproduction. As a first step towards solving the VN puzzles, we measure the angular differential cross section $d\sigma/d\Omega$ at incident pion momenta ranging from 1.6 to 2.4 GeV/c for $\pi^- p \to \phi n$, of which current experimental data are obviously quite limited. In this measurement, we plan to use secondary pions (≈ 10 kHz) delivered at the high-p beamline with a 400-W loss of the primary proton beam at the Lambertson magnet. We expect to obtain a few thousand $\phi \to K^+K^-$ events at a fixed incident momentum in 10-days measurement. We utilize the spectrometer magnet for the E16 experiment in process to study the spectral change of ϕ mesons in a nucleus by detecting e^+e^- pairs from the ϕ decay, We combine the detectors system for the E16 experiment and

that developed for the E50 experiment aiming at spectroscopy of charmed baryons using the $\pi^- p \to D^{*-} Y_c^{*+}$ reaction. We request 10-days measurement at each incident momentum from 1.6, 1.8, 2.0, 2.2, and 2.4 GeV/c, and additional 5-days commissioning of the combined E16 and E50 detector system.

I. INTRODUCTION

Hadrons are composite particles consisting of quarks and gluons. The strong interaction between them is provided in the fundamental theory, quantum chromodynamics (QCD). Nevertheless, the dynamics of hadrons is difficult to be described from the interactions between quarks and gluons. Neither quarks nor gluons are direct effective degrees of freedom (building blocks) of hadrons. Instead, dressed quarks (constituent quarks) and Nambu-Goldstone bosons (such as pions), emerging from the chiral symmetry breaking, form the building blocks of hadrons. Several models incorporating them well-reproduce not only the properties of the ground-state hadrons [1, 2] but also the important features of the interaction between nucleons (nuclear force) [3, 4]. Simply describing "quark" instead of "constituent quark," familiar hadrons are classified into mesons containing a quark-antiquark pair ($q\bar{q}$) and baryons containing three quarks (qqq). And excited hadrons are considered as radial and orbital excitations of the ground-state hadrons. However, disagreement has been recognized between experimental results and theoretical calculations for highly excited (or high-mass) hadrons described with the constituent quarks [5]. Especially the so-called exotic hadrons receive a particular interest since they are comprised of more than three quarks such as the P_c pentaquark baryons observed in the $J/\psi p$ invariant-mass distributions by the LHCb collaboration [6, 7].

Phenomena beyond the hadron description in terms of constituent quarks appear not only in spectroscopy of hadrons but also in hadron-hadron interactions. Let us focus on systems between a vector meson and nucleon. There exist several puzzles in the ϕN and $J/\psi N$ systems, which we call the vector-meson and nucleon (VN) puzzles, and major three issues are as follows:

1. ϕ photoproduction on the proton shows an unidentified bump at 2.2 GeV in $d\sigma/dt|_{t=-|t|_{\rm min}}$ as a function of the center-of-mass (CM) energy (W) [8–10],

2. J/ψ photoproduction on the proton does not show any peaks corresponding to the P_c pentaquark baryons [11], and

3. ϕ photoproduction experiments provide completely different scattering lengths [12] from those determined in other methods [13, 14].

Let us discuss these issues in the following subsections.

A. Unidentified bump at $W = 2.2$ GeV in $\gamma p \to \phi p$

The ϕ meson is an almost pure $s\bar{s}$ state. The Okubo-Zwieg-Iizuka (OZI) rule makes the interaction of the ϕ meson to the nucleon weak owing to little admixture of $s\bar{s}$ in the nucleon wave function. Thus, resonances have not been considered between ϕ and the nucleon. However, a bump was observed at $W = 2.2$ GeV in $d\sigma/dt|_{t=-|t|_{\rm min}}$ as a function of W for ϕ photoproduction on the proton ($\gamma p \to \phi p$) [8–10]. Figure 1(left) shows $d\sigma/dt|_{t=-|t|_{\rm min}}$ as a function of W for $\gamma p \to \phi p$. A bump is clearly observed at $W = 2.2$ GeV corresponding to the incident photon energy of $E_\gamma \approx 2.0$ GeV.

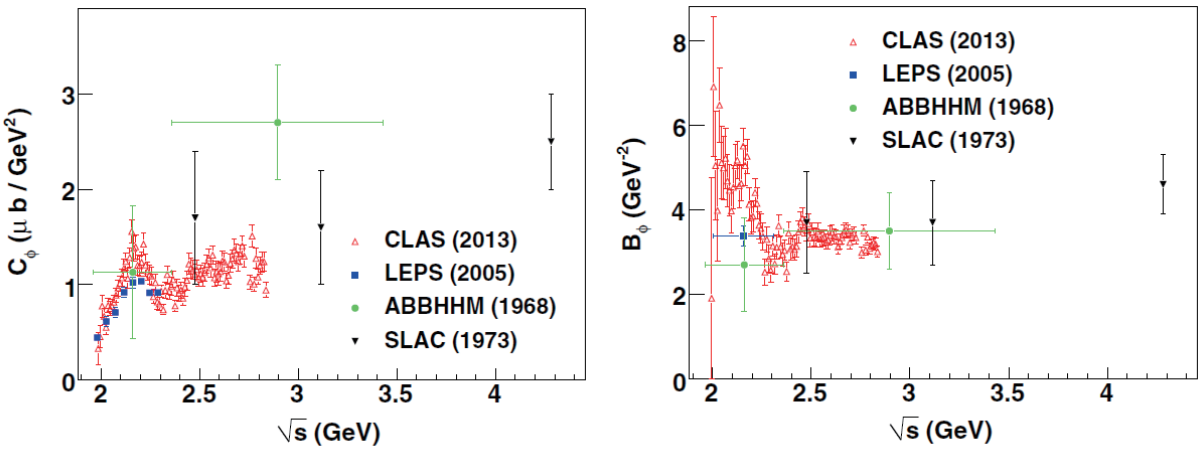

FIG. 1. C_ϕ (left) and B_ϕ (right) as a function of W (the figure is taken from Ref. [9]). The parameters C_ϕ and B_ϕ are determined by fitting a function expressed in Eq. (1) to the differential cross section $d\sigma/dt$ at each incident photon energy. C_ϕ corresponds to $d\sigma/dt$ at $t = -|t|_{\rm min}$. A bump is observed at $W = 2.2$ GeV in $C_\phi(W)$, and a sudden drop is observed in $B_\phi(W)$ at the same location as the bump in $C_\phi(W)$.

Photoproduction of ϕ mesons dominantly takes place in the t-channel exchange of multi-gluons within the vector-meson dominance (VMD) model. As shown in Fig. 2, incident photons are converted into ϕ mesons, and elastic scattering occurs on the nucleon by exchanging a Pomeron (multi-gluons). This t-channel dominance leads to a forward-peaking angular distribution of the produced ϕ mesons. The differential cross sections $d\sigma/dt$ is well fitted with the following exponential function:

$$\frac{d\sigma}{dt} = C_\phi \exp\left\{B_\phi \left(t + |t|_{\rm min}\right)\right\} \tag{1}$$

at a certain incident photon energy. Here, C_ϕ corresponds to $d\sigma/dt$ at $t = -|t|_{\rm min}$, and B_ϕ denotes the exponential slope of $d\sigma/dt$ as shown in Fig. 1(right). A sudden change of B_ϕ is observed at $W = 2.2$ GeV, where the bump is observed in $C_\phi(W)$ as shown in Fig. 1(left).

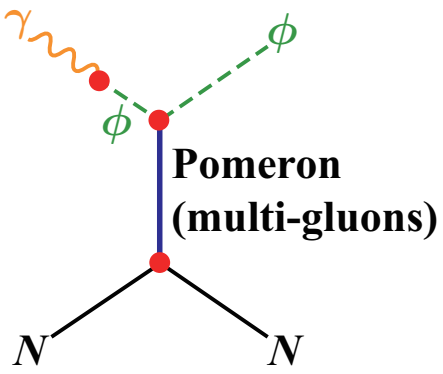

FIG. 2. Dominant diagram for $\gamma p \to \phi p$. Incident photons are converted into ϕ mesons, and elastic scattering occurs on the nucleon by exchanging a Pomeron (multi-gluons).

The origin of the bump in $C_\phi(W)$ has been widely studied. A possibility was discussed that a nucleon resonance $N(2080)3/2^-$ (D_{13}) forms this bump [15]. However, it appears only at forward angles [9], indicating that a conventional resonance interpretation seems inappropriate. Alternatively, the ϕ-$\Lambda(1520)$ interference was considered that the final-state K^+K^-p particles are the same between the $\gamma p \to \phi p$ and $\gamma p \to K^+\Lambda(1520)$ reactions. However, the interference effect does not account for the bump since it has been also observed in the neutral mode of ϕ photoproduction ($\gamma p \to K^0_S K^0_L p$) [16] and since the relative phase between ϕ and $\Lambda(1520)$ does not form the bump [17].

Various hadronic rescattering contributions in ϕ photoproduction are discussed in Ref. [18]. Although the bump structure at $W = 2.2$ GeV in $C_\phi(W)$ could be explained by $K^+\Lambda(1520)$ rescattering in the intermediate state, B_ϕ cannot be reproduced by this rescattering effect. As a result of the OZI rule, ϕ photoproduction takes place via multi-gluon exchange (Pomeron trajectory) with $J^{PC} = 0^{++}$, showing a monotonically increasing $C_\phi(W)$. The bump cannot be reproduced even if incorporated is the non-perturbative two-gluon-exchange dynamics [19] or the manifestation of a daughter Pomeron trajectory [20].

At present, the origin of the bump at 2.2 GeV in $C_\phi(W)$ is not clear. A conventional resonance interpretation was earlier considered inappropriate for the bump observed in pho-

toproduction. Contributions from s-channel ϕN resonances to the bump can not be completely rejected since ϕ photoproduction is insensitive to them. The differential cross section $d\sigma/dt$ at a fixed E_γ (fixed W) shows a strong exponential behavior from the threshold as shown in Fig. 3, or $B_\phi \gg 0$ from the threshold as shown in Fig. 1(right). Owing to the OZI rule, the dominant mechanism in ϕ photoproduction is a diffractive process as shown in Fig. 2, and contributions from s-channel ϕN resonances would be highly suppressed.

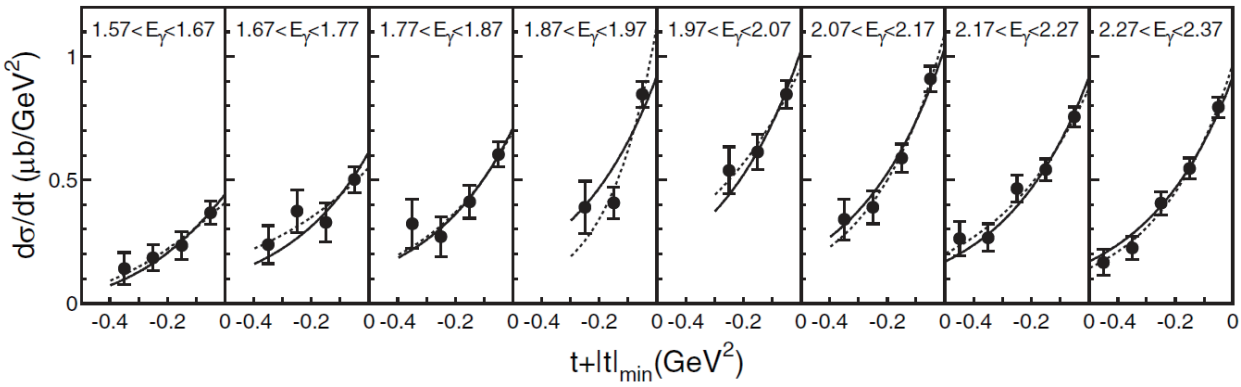

FIG. 3. Differential cross sections $d\sigma/dt$ as a function of $t' = t + |t|_{\rm min}$ for $\gamma p \to \phi p$ (the figure is taken from Ref. [8]). The curves indicate the fitted functions in Eq. (1). The dashed curves show those with free B_ϕ parameters, and the solid with a fixed $B_\phi = 3.38$ GeV$^2/c^2$.

The dominant process of the $\pi^- p \to \phi n$ reaction is expected to be the formation of the s-channel resonance as shown in Fig. 4. The $\pi^- p \to \phi n$ reaction gives relatively uniform angular distributions ($d\sigma/dt$ as a function of t) as shown in the next section, suggesting that the t-channel exchange is highly suppressed. Fig. 5 shows the total cross sections for $\pi^- p \to \phi n$ calculated with ρ and π exchanges [21]. The enhancement from the calculation at low energies ($s/s_{\rm th} < 2$) comes from missing contributions from s-channel resonances. Here, $s_{\rm th}$ denotes s at the threshold $(M_n + M_\phi)^2$. It could be concluded that the s-channel dominance in $\pi^- p \to \phi n$ for $s/s_{\rm th} < 2$. The $\pi^- p \to \phi n$ reaction is an ideal reaction to investigate nucleon resonances (N^*s) coupling to ϕN and a possible exotic state coupling to ϕN, which will be discussed in the next subsection.

In principle, any nucleon resonance (N^*) with a mass around 2.05 GeV is a candidate of the intermediate states for ϕN production. The S-wave ϕN system gives a spin-parity of $1/2^-$ and $3/2^-$, and N^*s with $1/2^-$ or $3/2^-$ may be likely to couple to ϕN. The nucleon resonance $N(2080)3/2^-$ (D_{13}) is a candidate N^* [15]. Oset and Ramos discuss dynamically

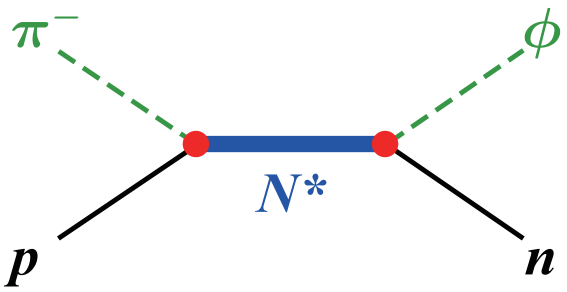

FIG. 4. Dominant diagram for $\pi^- p \to \phi n$. The s-channel resonances, nucleon resonances (N^*s) or exotic state coupling to ϕN, appear in the intermediate state.

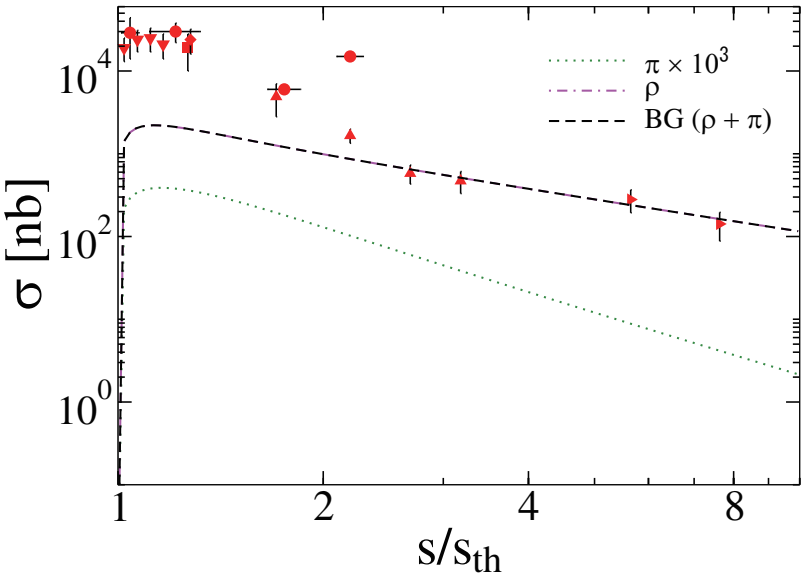

FIG. 5. Total cross sections for $\pi^- p \to \phi n$ calculated with ρ and π Reggeon exchanges (the figure is taken from Ref. [21]). The enhancement over the calculation comes from missing s-channel contributions. Here, $s_{\rm th}$ denotes s at the threshold $(M_n + M_\phi)^2$.

generated resonances from the ϕN interaction, finding a resonance coupling to ϕN has a mass of 2.035 GeV [22, 23]. However, this resonance couples more strongly to $K^*\Sigma$. Measurements of cross sections for $\pi^- p \to \phi n$ is quite important for the systematic studies of N^*s coupling to ϕN. It should be noted that no N^*s coupling to ϕN are listed currently in the Review of Particle Physics [24].

B. Non observation of the P_c pentaquark baryons in $\gamma p \to J/\psi p$

Recently, hidden-charm P_c baryons, $P_c(4312)^+$, $P_c(4440)^+$, and $P_c(4457)^+$, are reported by the LHCb collaboration, which are observed in the $J/\psi p$ invariant-mass distributions for the $\Lambda_b \to J/\psi p K^-$ decay [6, 7] as shown in Fig. 6. These P_c baryons could be a spatially-compact pentaquark object ($qqqq\bar{q}$) including hidden charm ($c\bar{c}$) and/or a meson-baryon molecule-like state ($\Sigma_c^+ \bar{D}^0$ or $\Sigma_c^+ \bar{D}^{*0}$). If a P_c baryon really exists, it should show up independently of the initial state of reactions. The GlueX collaboration measures the total cross section as a function of E_γ for J/ψ photoproduction on the proton ($\gamma p \to J/\psi p$) [11]. No peaks are observed corresponding to the P_c baryons reported by the LHCb collaboration. There is a possibility that the small branching ratio of $P_c \to J/\psi p$ makes it difficult to observe them in photoproduction. Still not definitely settled is what is the structure of the P_c baryons [25–27].

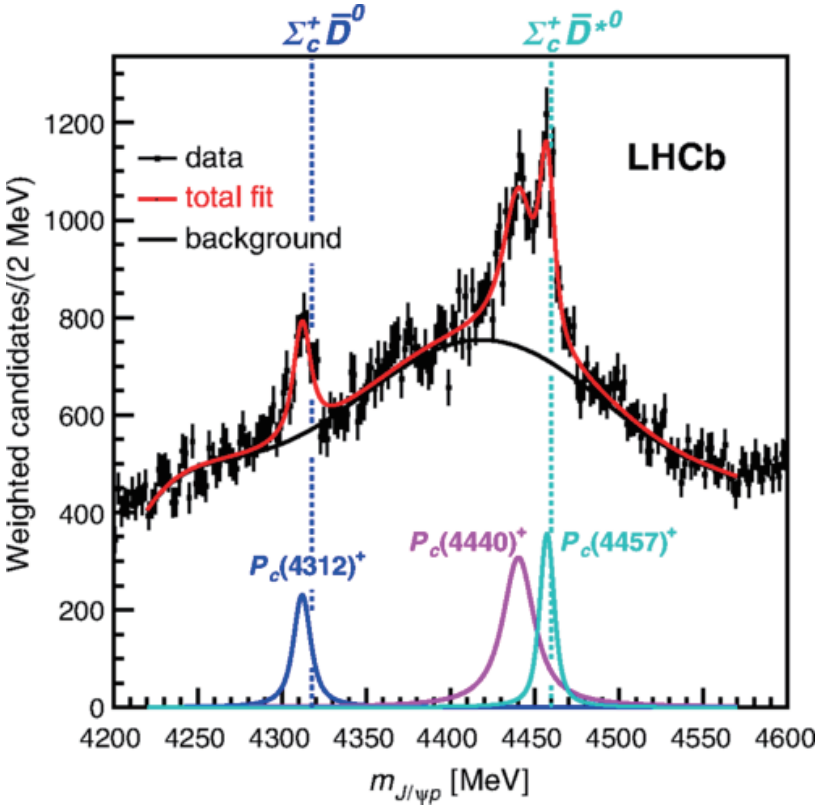

FIG. 6. $J/\psi p$ invariant-mass distribution for the $\Lambda_b \to J/\psi p K^-$ decay taken from Ref. [7]. Three peaks corresponding to pentaquark baryons are observed just below the $\Sigma_c^+ \bar{D}^0$ and $\Sigma_c^+ \bar{D}^{*0}$ thresholds.

The J/ψ meson is a pure $c\bar{c}$ state similarly to the fact that ϕ is an almost pure $s\bar{s}$ state. The OZI rule makes the interaction of a J/ψ meson to the nucleon weak owing to little admixture of $c\bar{c}$ in the nucleon wave function. Thus, it is difficult to consider P_c baryons as ordinary J/ψ-nucleon resonances, and P_c baryons would be exotic pentaquark states. The unidentified bump observed in ϕ photoproduction [8–10] has similar conditions to P_c baryons. Both of them include hidden strangeness or hidden charm. P_c baryons are located at $\Sigma_c^+\bar{D}^0$ and $\Sigma_c^+\bar{D}^{*0}$ thresholds, and the bump observed in ϕ photoproduction is close to the $K^+\Lambda(1520)$ and $K^{*+}\Lambda$ thresholds. Thus, the bump observed in ϕ photoproduction could be an exotic pentaquark state having hidden strangeness, and we call this possible exotic state P_s. Studying ϕN resonances via the $\pi^- p \to \phi n$ reaction is important not only for identifying hidden-strangeness baryons but also revealing the structure of the P_c baryons. Possible open-charm exchange in J/ψ photoproduction gives step-like structure in the total cross-section as a function of the CM energy [28]. The $d\sigma/dt$ is expected to be flat due to the heavy particle exchange, $D\Lambda_c$, unlike that for the two-gluon exchange. This is similar to the open-strange exchange, $K^+\Lambda(1520)$, in ϕ photoproduction. In addition to $\pi^- p \to \phi n$, $\pi^- p \to J/\psi n$ is an important reaction (yet to be investigated) to study P_s and P_c baryons.

C. Different ϕN scattering lengths obtained from different methods

Thus far, the ϕN interaction has not been considered to be strong [29–31] enough producing a resonance except for that in the nuclear medium [32]. Recently, Strakovsky *et al.* precisely extracted the absolute value of the scattering length $|a_{\phi N}| = 0.063 \pm 0.010$ from ϕ photoproduction on the proton ($\gamma p \to \phi p$) near the threshold assuming a vector-meson dominance (VMD) model [12]. The extracted value is consistent with a weak ϕN interaction. More recently, two particle correlation in the pp collision suggests an attractive ϕp interaction [13]. The scattering length $a_{\phi N}$[1] obtained is $(0.85 \pm 0.34 \pm 0.14) + i\,(0.16 \pm 0.10 \pm 0.09)$ fm in the Lednický-Lyuboshits approach [33], which seems inconsistent with the previous values. A lattice QCD calculation also obtains attractive scattering length $a_{\phi N}^{3/2} =$

[1] We define the scattering length $a_{\phi N}$ and effective range $r_{\phi N}$ through an effective-range expansion of the S-wave phase shift $\delta(p)$ as

$$p \cot \delta(p) = \frac{1}{a_{\phi N}} + \frac{1}{2}\, r_{\phi N}\, p^2 + O(p^4), \tag{2}$$

where p denotes the momentum of ϕ in the ϕN CM frame. In this definition, a positive (negative) Re $a_{\phi N}$ gives attraction (repulsion or attraction with the existence of a bound state), and a positive Im $a_{\phi N}$ corresponds to the absorption to another channel.

$1.43 \pm 0.23^{+0.36}_{-0.06}$ fm only for the spin 3/2 channel [14]. This value is also completely different from the weak ϕN interaction. Although the strength of the ϕN interaction is still controversial, strong attraction for producing a resonance might be expected.

It seems that only the scattering length obtained from ϕ photoproduction is smaller than that from each of the other methods. In photoproduction, ϕ mesons scattering on the nucleon are not in equilibrium. Suppression in ϕN interaction close to threshold may be observed because of $s\bar{s}$ pair in point-like configuration lacks sufficient time to form complete ϕ wave function. This effect is called the "young" meson effect, and is discussed in Ref. [34]. An alternative interpretation is provided in formalism of Dyson-Schwinger equations [35]. Additionally, virtual ϕ mesons converted from incident photons are quite far from onshell. This offshellness may make it difficult to determine the scattering length phenomenologically by using VMD.

As discussed in subsection I A, it is difficult to extract the S-wave ϕN scattering contribution in ϕ photoproduction. The ϕN scattering length and effective range can be obtained from the shape of the total cross section for $\pi^- p \to \phi n$ as a function of the incident pion momentum using the scattering equation with final-state interactions similarly to Ref. [36]. Here, it is necessary to perform high-precision measurement of the total cross section with fine binning of the incident pion momentum. This is the second step of the $\pi^- p \to \phi n$ measurements.

II. $\pi^- p \to \phi n$ REACTION

To investigate s-channel ϕN resonances or S-wave ϕN scattering, information on the $\pi^- p \to \phi n$ reaction is definitely crucial. Therefore, we plan to measure the total and differential cross sections of this reaction near the threshold (at incident pion momenta below 2.4 GeV/c). Additionally, $\pi^- p \to \phi n$ is one of the elementary processes of ϕ production. The measured cross sections are an important input for ϕ production in the pA collision for investigating the medium modification of the ϕ properties [37, 38].

A. Existing data

At present, available $\pi^- p \to \phi n$ data are quite limited [39–45]. Figure 7 shows the total cross section as a function of the incident pion momentum. A large cross sections around 20–30 μb are given near the threshold even though the measurements were not performed in a fine step of the incident momenta. Above the incident pion momentum (P_π) of 3 GeV/c, a rapid decrease of the cross section as a function of P_π in an exponential form. Table I summarizes the measured total cross sections and the number of the ϕ- or K^+K^--produced events. Except for Ref. [45], total cross sections were measured before 1980, and their uncertainties are large owing to poor statistics (the number of ϕ- or K^+K^--produced events are much less than 1,000).

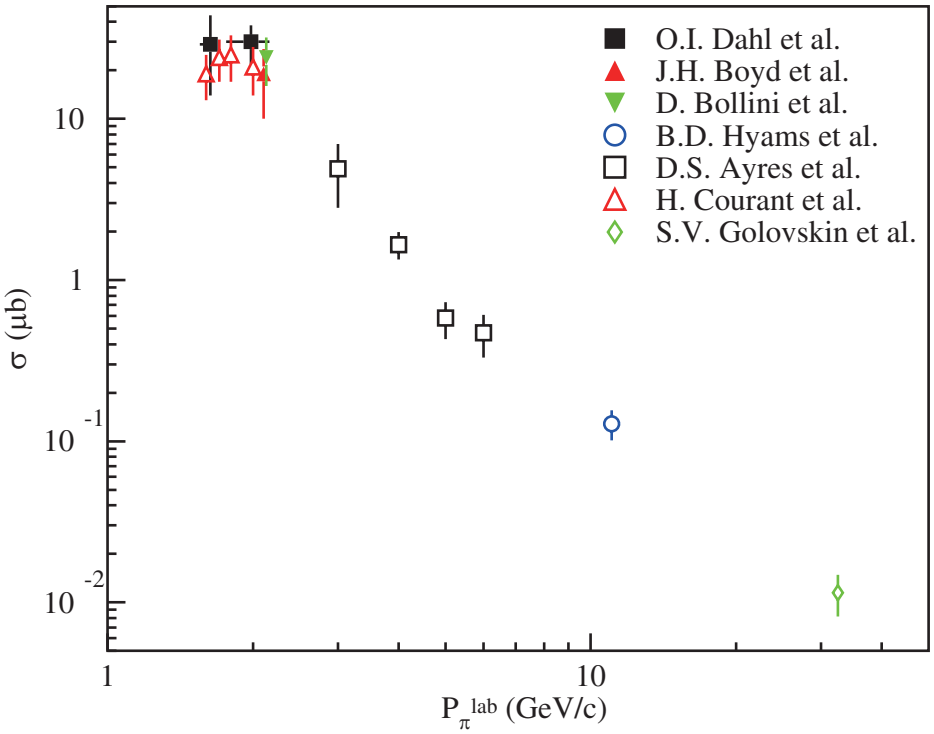

FIG. 7. Total cross section as a function of the incident pion momentum. The cross section data are not precisely determined for the resonance region ($P_\pi \approx 2$ GeV/c). The different markers come from different experiments, which are described in the panel.

It is difficult to investigate the intermediate ϕN resonances in detail owing to the lack of total and differential cross-section data in the resonance region ($P_\pi \approx 2$ GeV/c). However, the available data tell us the order of the production cross section. The total cross sections

TABLE I. Measured total cross sections and the number of the ϕ- or K^+K^--produced events. The data are summarized with respect to the incident pion momentum (P_π) for each reference. At higher incident momenta, a large background contribution appears in the K^+K^- invariant-mass distribution, the uncertainties of the numbers of the ϕ-produced events, and those of total cross sections are large.

Reference	P_π (GeV/c)	σ_ϕ (μb)	#events
O.I. Dahl *et al.* (1967) [39]	1.58–1.71	29 ± 15	40 ϕ (84 KK)
	1.8–2.2	30 ± 8	
	2.58–2.63	0 ± 9	
	2.9–3.3	6 ± 8	
	3.8–4.2	15 ± 20	
J.H. Boyd *et al.* (1968) [40]	2.1	10^{+9}_{-8}	95 KK
D. Bollini *et al.* (1969) [41]	2.13	24 ± 8	82 ± 25 ϕ
B.D. Hyams *et al.* (1970) [42]	11.04	$0.128^{+0.027}_{-0.028}$	
D.S. Ayres *et al.* (1974) [43]	3	4.9 ± 2.1	300 ϕ
	4	1.66 ± 0.32	
	5	0.58 ± 0.15	
	6	0.47 ± 0.14	
H. Courant *et al.* (1977) [44]	1.6	19 ± 6	23 ϕ
	1.7	24 ± 7	38 ϕ
	1.8	25 ± 8	80 ϕ
	2.0	21 ± 7	28 ϕ
S.V. Golovskin *et al.* (1997) [45]	32.5	0.0115 ± 0.0033	1670 ± 410 ϕ

measured are 20–30 μb at $P_\pi \approx 2$ GeV/c although they are not precisely determined. The data also tell us that the t-channel process is highly suppressed at $P_\pi \approx 2$ GeV/c. Figure 8 shows the differential cross sections $d\sigma/dt'$s for $\pi^- p \to \phi n$, $K^- p \to \phi\Lambda$, and $K^- p \to \phi\Sigma^0$, where t' denotes $t + |t|_{\rm min}$. The B_ϕ slope parameters obtained are 0.4 ± 1.8, 0.1 ± 0.5, 1.2 ± 0.4, and 1.6 ± 0.6 GeV$^2/c^2$ at $P_\pi = 3$, 4, 5, and 6 GeV/c, respectively, when an

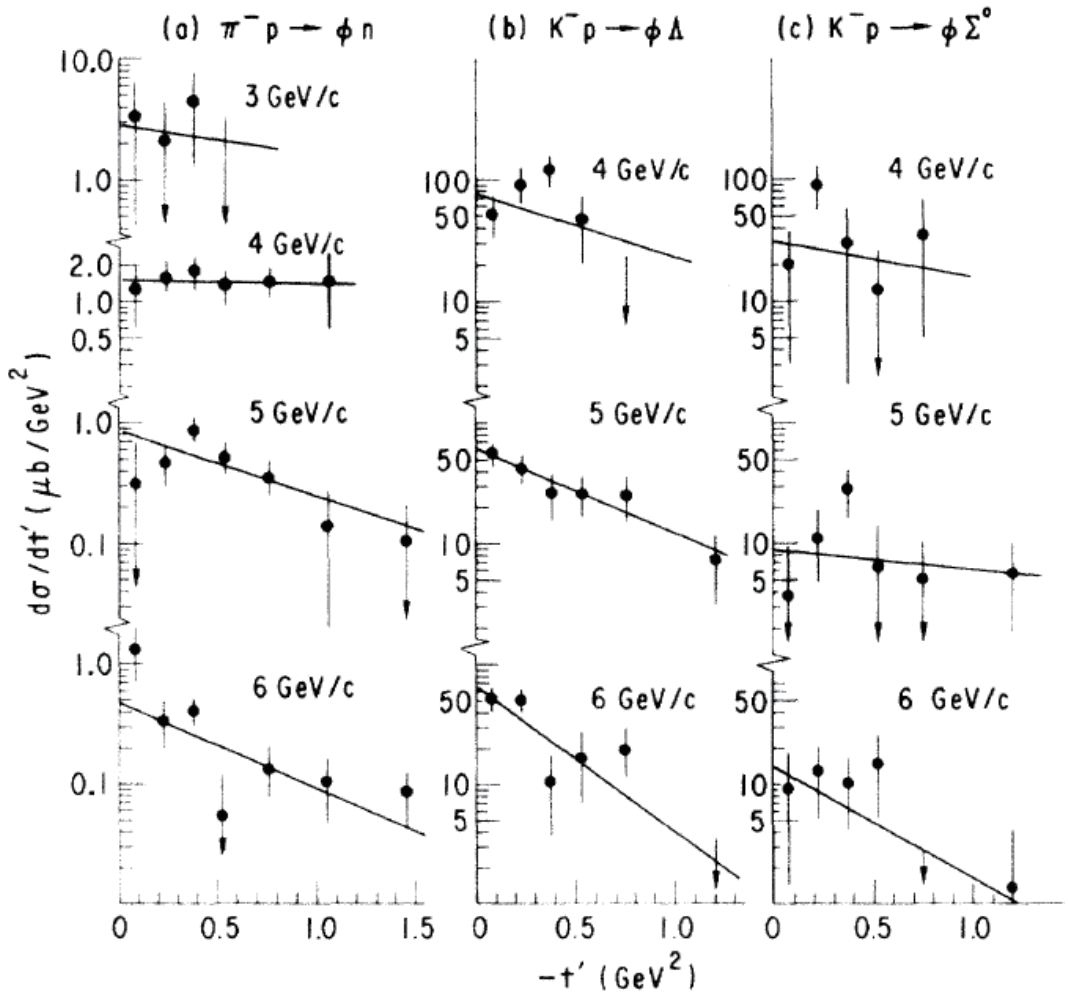

FIG. 8. Differential cross sections $d\sigma/dt'$ for $\pi^- p \to \phi n$ (a), and other reactions (th figure is taken from Ref. [43]). The lines show the fitted $d\sigma/dt' = C_\phi \exp(B_\phi t')$ function. Here t' denotes $t + |t|_{\rm min}$.

exponential function

$$\frac{d\sigma}{dt'} = C_\phi \exp(B_\phi t') \tag{3}$$

is fitted to the $\pi^- p \to \phi n$ data. It should be noted that Eqs. (1) and (3) are equivalent and C_ϕ and B_ϕ parameters are the same between these equations. Below $P_\pi = 4$ GeV/c, $d\sigma/dt'$ does not show a strong exponential behavior ($B_\phi \approx 0$), suggesting a rather uniform $d\sigma/d\Omega$ angular distribution in the CM frame. On the contrary, $d\sigma/dt'$ shows a strong exponential behavior (a finite B_ϕ) from the reaction threshold ($E_\gamma = 1.57$ GeV) in photoproduction as shown in Fig. 3. Therefore, the $\pi^- p \to \phi n$ reaction is suitable for studying possible ϕN resonances, or S-wave ϕN scattering. It should be noted that a strong exponential behavior

is observed in the $K^- p \to \phi\Lambda$ or $K^- p \to \phi\Sigma^0$ reaction where the K-exchange process is expected to be dominant.

We plan to measure cross sections of $\pi^- p \to \phi n$ at incident pion momenta from 1.6 to 2.4 GeV/c with a 0.2 GeV/c step at the high-intensity high-momentum secondary beamline at J-PARC. Our measurement primarily aims at confirming whether the same bump is observed or not in $\pi^- p \to \phi p$ as in $\gamma p \to \phi p$. Since the momentum bite of the beamline is expected to be $\pm 2\%$, the 1.6-GeV/c data include the incident pion momenta ranging from 1.57 to 1.63 GeV/c, which provide cross sections at the vicinity of the threshold (especially below 1.58 GeV/c) for the first time. Taking these data with high statistics lead to the determination of the low-energy ϕN scattering parameters as discussed later in Appendix D.

B. Expected cross sections

We have calculated the cross sections for $\pi^- p \to \phi n$ and confirmed that the enhancement $s/s_{\rm th} < 2$ or $W < 2.4$ GeV comes from s-channel ϕN contributions. Figure 9 shows the diagram of $\pi^- p \to \phi n$ for calculating cross sections. The diagram of interest is the s-channel contributions of nucleon resonances and possible P_s pentaquark baryon with hidden strangeness shown in Fig. 9(a). The main background contribution is the t-channel exchange of ρ^+ and π^+ mesons shown in Fig. 9(b). Since the branching ratio of $\phi \to \rho^+\pi^-$ ($15.4\% \pm 0.4\%$) is much higher than that of $\phi \to \pi^+\pi^-$ ($(7.3 \pm 1.3) \times 10^{-5}$), the contribution from the ρ exchange is much larger than that from the π. We have also considered box diagrams shown in Figs. 9(c) and (d). In general, contributions from these diagrams are expected to

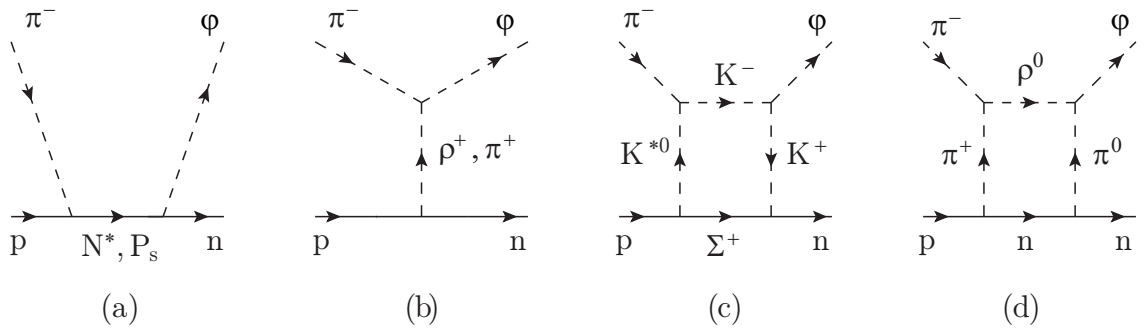

FIG. 9. Diagram of $\pi^- p \to \phi n$ for calculating cross sections. (a) s-channel contribution (N^* and P_s intermediate states). (b) t-channel contribution (ρ and π exchanges). (c) and (d) box diagrams.

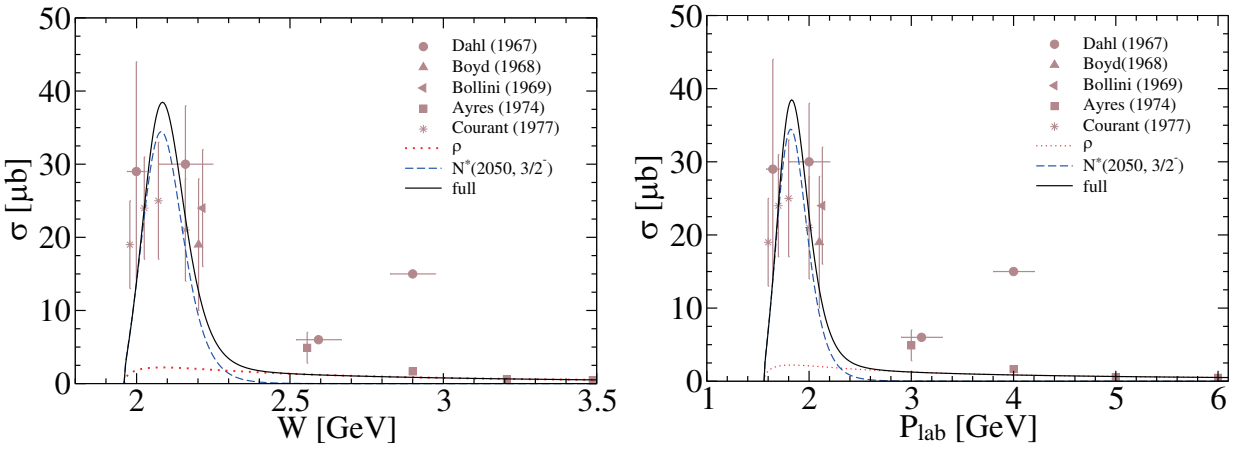

FIG. 10. Total cross section as a function of the center of mass energy W (left), and that as as a function of the incident pion momentum P_π (right). The solid curve shows the calculated total cross section (full). The blue dashed and red dotted curves represent the contributions from the two major contributions, ρ exchange and $N(2050)3/2^-$ intermediate state, respectively.

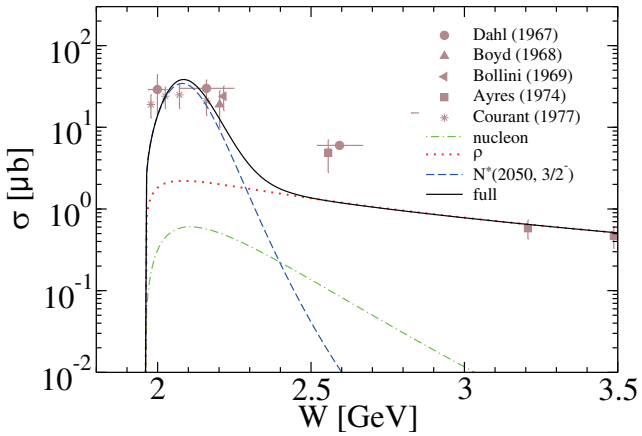

FIG. 11. Total cross section as a function of W where the s channel nucleon contribution is incorporated. The green long-dashed curve represent the s-channel nucleon contribution. The other legends are the same as those in Fig. 10.

be very small.

At first, adopted are the same model parameters in Ref. [21] for π and ρ exchanges to reproduce the total cross sections above $W = 3$ GeV where t-channel contributions are dominant. Additionally, assumed is an N^* resonance with a mass of 2.05 GeV, a width of 0.3 GeV, and a spin-parity of $3/2^-$ so that the total cross section below $W = 3$ GeV

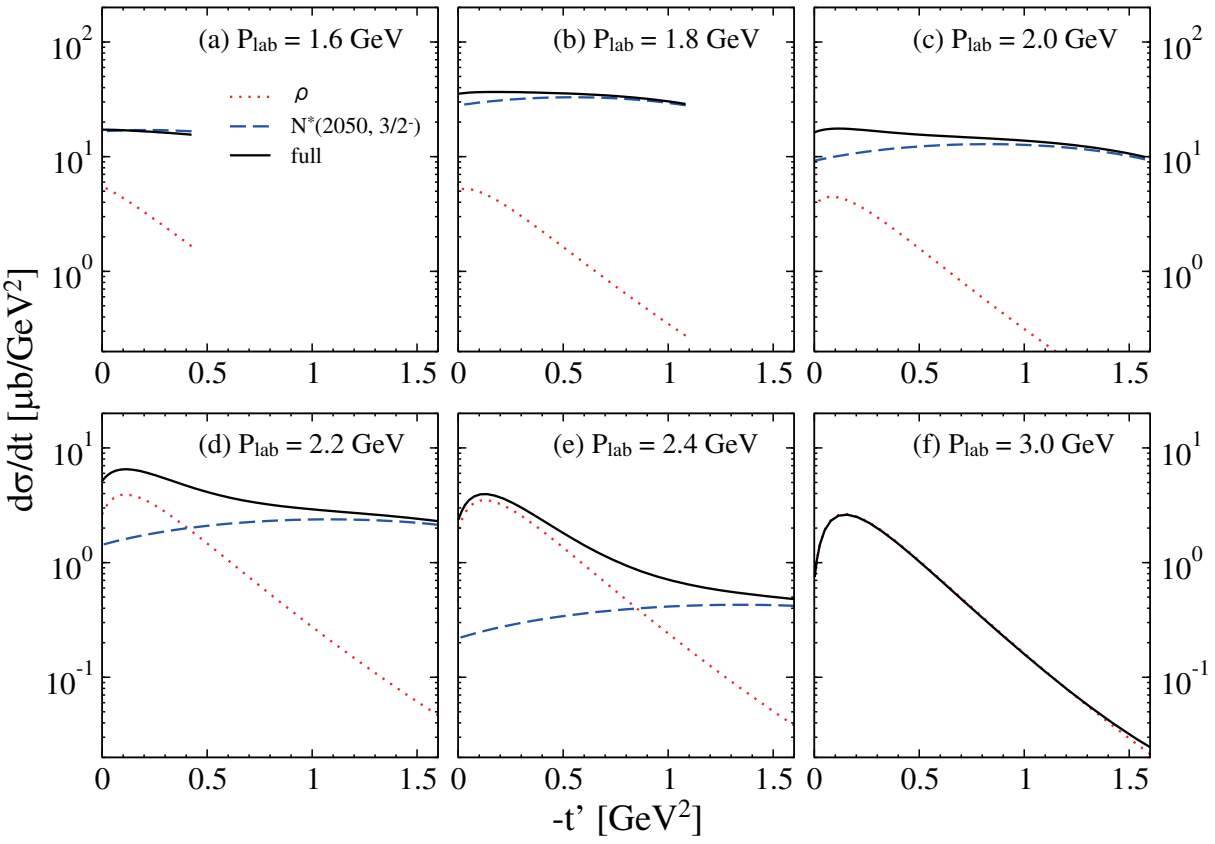

FIG. 12. Differential cross section $d\sigma/dt$ as a function of $-t'$ where t' denotes $t + |t|_{\rm min}$. The solid curve shows the $d\sigma/dt$ in the full calculations. The blue dashed and red dotted curves represent the contributions from the ρ exchange and $N(2050)3/2^-$ intermediate state, respectively.

could be roughly reproduced. The N^* or P_s contribution near the threshold is necessary for explaining the cross sections. Figure 10(left) shows the total cross section as a function of W, and Figure 10(right) shows that as a function of the incident pion momentum P_π. The t-channel contribution is dominant above $W = 3.0$ GeV ($P_\pi = 4.3$ GeV/c), and the s-channel contribution is dominant below $W < 2.6$ GeV ($P_\pi = 3.1$ GeV/c).

The enhancement of total cross section below $W = 2.6$ GeV shows that the s-channel contribution is dominant near the threshold. However, not only nucleon resonances but also nucleon could contribute to the s channel. We also calculate the total cross section by including the s-channel nucleon contribution. Here, the admixture of $s\bar{s}$ in the proton is assumed to be 1%. Figure 11 shows the total cross section as a function of W where the s-channel nucleon contribution is incorporated. Since the s-channel nucleon contribution is very small, the enhancement near the threshold must comes from nucleon resonances or

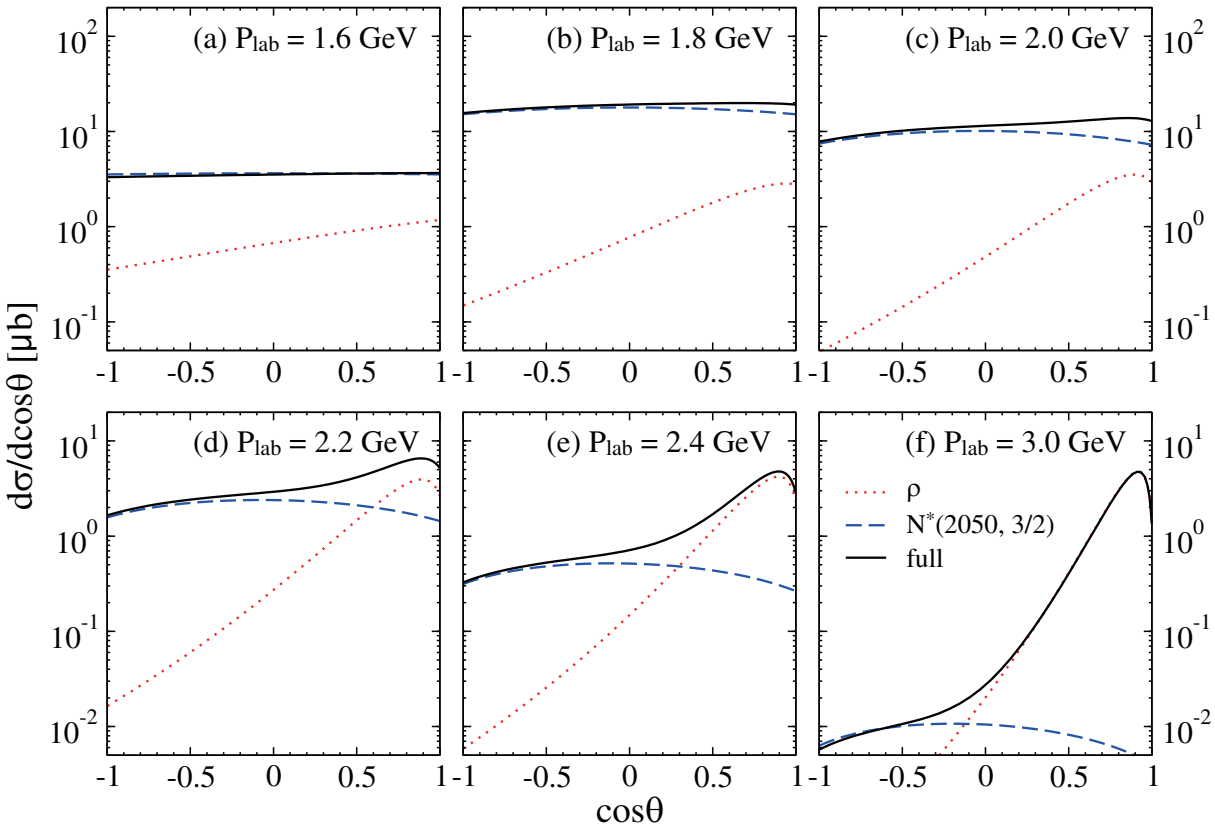

FIG. 13. Differential cross section $d\sigma/d\cos\theta$ as a function of $\cos\theta$, where θ denotes the emitted (polar) angle of ϕ mesons in the center-of-mass frame. The legends are the same as those in Fig. 12.

possible pentaquark state.

Since the s-channel nucleon contribution is negligibly small, we omit it in calculating differential cross sections. We use 1.6, 1.8, 2.0, 2.2, and 2.4 GeV/c negative pions in the planned experiment, and calculate the differential cross sections at these incident momenta and at 3.0 GeV/c for the reference. Figure 12 shows the differential cross section $d\sigma/dt$ as a function of $-t'$ ($t' = t + |t|_{\rm min}$). The small $-t'$ region includes the forward angles of ϕ emission, and $-t' = 0$ corresponds to the ϕ emission angle of 0°. The $-t'$ coverage is small at low incident π^- momenta, and it becomes larger as increase of the incident momentum. The calculated $d\sigma/dt$ is rather flat below $P_\pi = 2.0$ GeV/c, and some enhancement, corresponding mainly to the ρ-exchange process, is observed at small $-t'$ above $P_\pi = 2.0$ GeV/c. At $P_\pi = 3.0$ GeV/c, the s-channel contribution is difficult to be recognized.

For the study of baryon resonances, the angular differential cross section $d\sigma/d\Omega$ as a function of $\cos\theta$ is much suited. Figure 13 shows the differential cross section $d\sigma/d\cos\theta$

as a function of $\cos\theta$. It should be noted that $d\sigma/d\cos\theta = (2\pi)\, d\sigma/d\cos\Omega$. Although, the enhancement near $\cos\theta \approx 1$ is observed above $P_\pi = 2.0$ GeV/c, the s-channel ϕN resonances can be extracted from $d\sigma/d\Omega$ at backward angles ($\cos\theta < 0$). Since they contribute to the $d\sigma/d\Omega$ symmetric with respect to $\cos\theta = 0$ except for their interferences.

C. Kinematics

The ϕ meson has a mass $M = 1019.461 \pm 0.016$ MeV, and a full width $\Gamma = 4.249 \pm 0.013$ MeV [24]. The incident π^- momentum is 1.5593 GeV/c corresponding to the reaction threshold for production of ϕ having the centroid mass. Here, 938.272081, 939.565413, and 139.57039 MeV are employed for masses of the proton, neutron, and charged pion, respectively. At first, we show the CM energy W in Fig. 14(a) as a function of the incident π^- momentum P_π assuming ϕ has its centroid mass. The W increases linearly as increase of P_π. Pion beams at incident momenta of 1.6–2.4 GeV/c provide Ws ranging from 1.96 to 2.33 GeV. We have also estimated the CM-energy coverage ΔW corresponding to momentum bite $\Delta P_\pi/P_\pi = \pm 2\%$ of incident pions as shown in Fig. 14(b). Above 1.6 GeV/c, ΔW also increases linearly as increase of P_π, and ranges from 0.03 to 0.04 GeV.

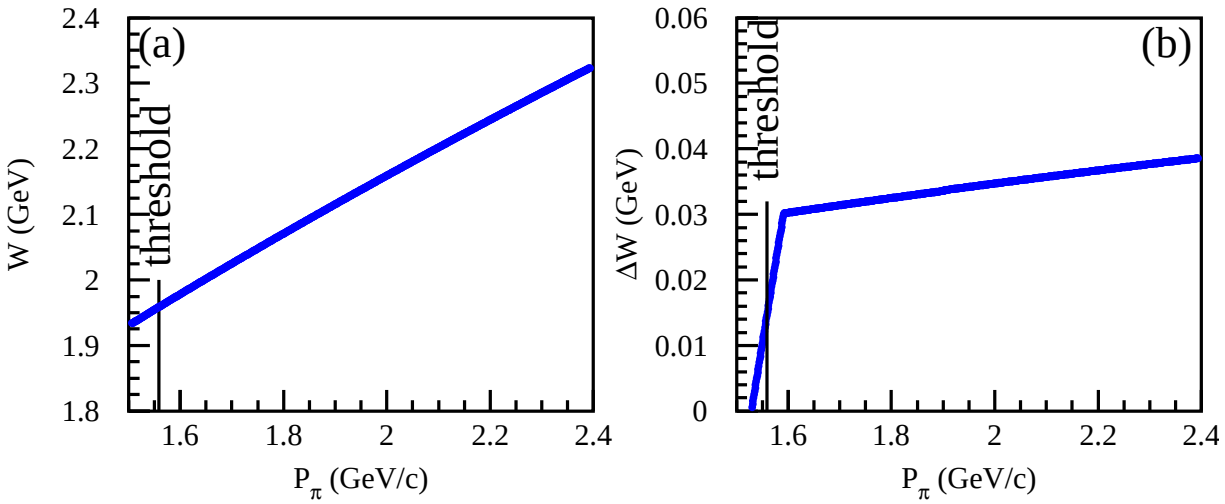

FIG. 14. (a) W as a function of P_π. (b) CM-energy coverage ΔW corresponding to the momentum bite $\Delta p/p = \pm 2\%$ of incident pions as a function of P_π.

Next, emitted angles and momenta of ϕs are discussed. Here, the mass of a produced ϕ meson is determined according to its centroid mass and full width. The generated events

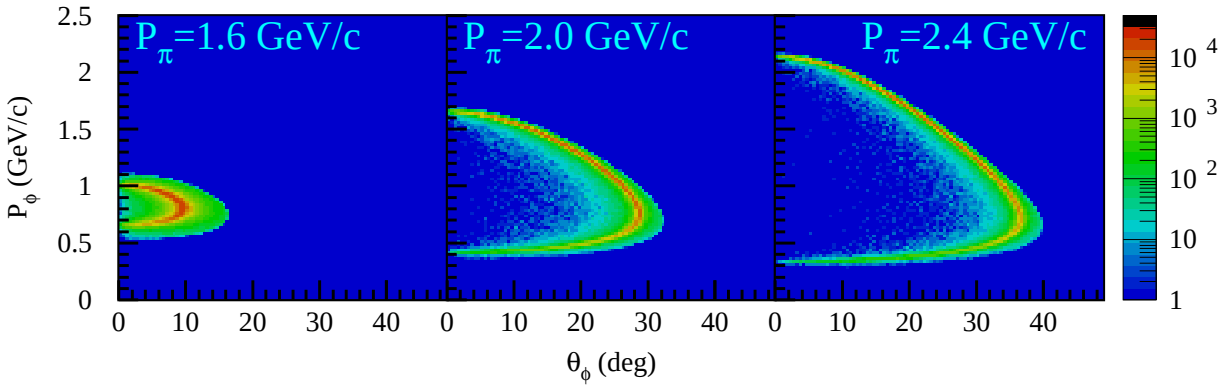

FIG. 15. P_ϕ as a function of θ_ϕ for ϕs in the laboratory frame. At $P_\pi = 2.4$ GeV/c, the maximum θ_ϕ is 40° and the maximum P_ϕ is 2.15 GeV/c.

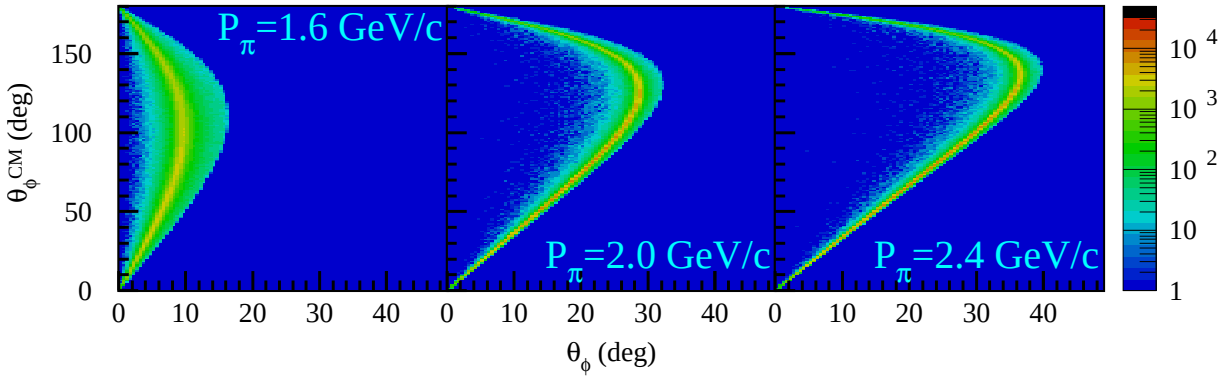

FIG. 16. Correlation of θ_ϕs between the CM frame and laboratory frame. Two θ_ϕs in the CM frame correspond to the same θ_ϕ in the laboratory frame.

are weighted by the phase volume of ϕn production with a certain ϕ mass. Fig 15 shows the momentum P_ϕ as a function of the emitted angle θ_ϕ for ϕs in the laboratory frame. The maximum θ_ϕ increases as increase of P_π. The maximum θ_ϕ is approximately 40° at $P_\pi = 2.4$ GeV/c. With increase of P_π, the maximum P_ϕ increases and the minimum P_ϕ decreases The minimum and maximum P_ϕs are 0.31 and 2.15 GeV/c at $P_\pi = 2.4$ GeV/c. Fig. 16 shows the correlation of θ_ϕs between the CM frame and laboratory frame.

Finally, we show the estimated emitted angles and momenta for kaons to be detected. Here, the generated ϕ meson is assumed to decay isotropically in the rest frame of ϕ into a K^+K^- pair. Fig. 17 shows the K emission angle θ_K as a function of θ_ϕ. The majority of the events makes θ_K proportional to θ_ϕ. This is because the ϕ mass is located near the K^+K^- threshold. The maximum θ_K also increases as increase of P_π. The maximum

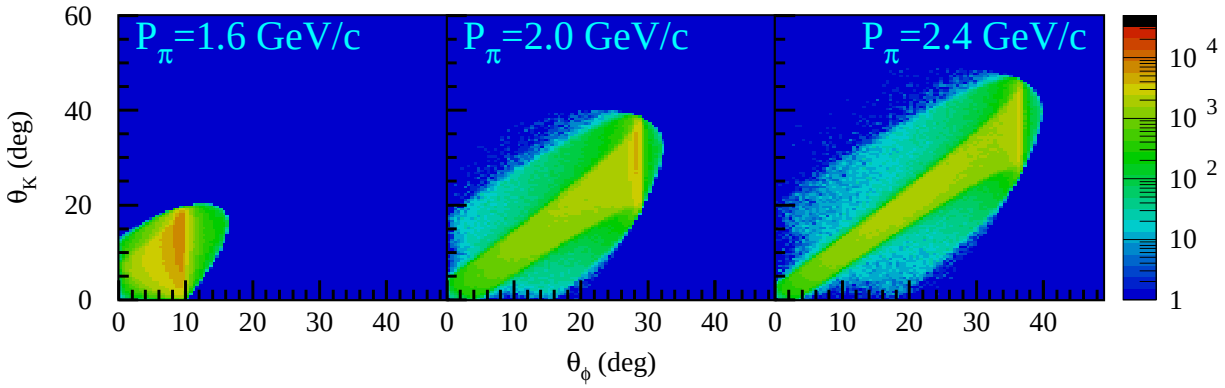

FIG. 17. K emission angle θ_K as a function of θ_ϕ. The majority of the events makes θ_K proportional to θ_ϕ and the maximum θ_K is approximately 49° at $P_\pi = 2.4$ GeV/c.

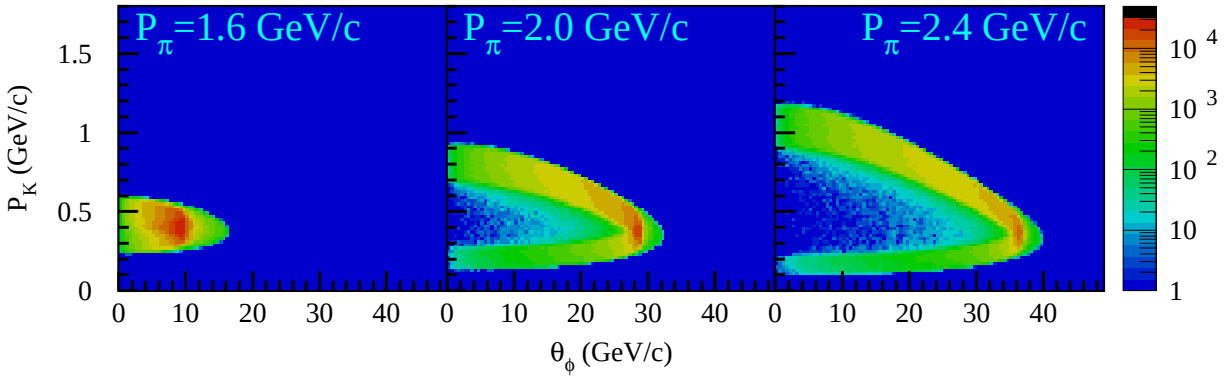

FIG. 18. K momentum P_K as a function of θ_ϕ. The maximum P_K is 1.19 GeV/c at $P_\pi = 2.4$ GeV/c.

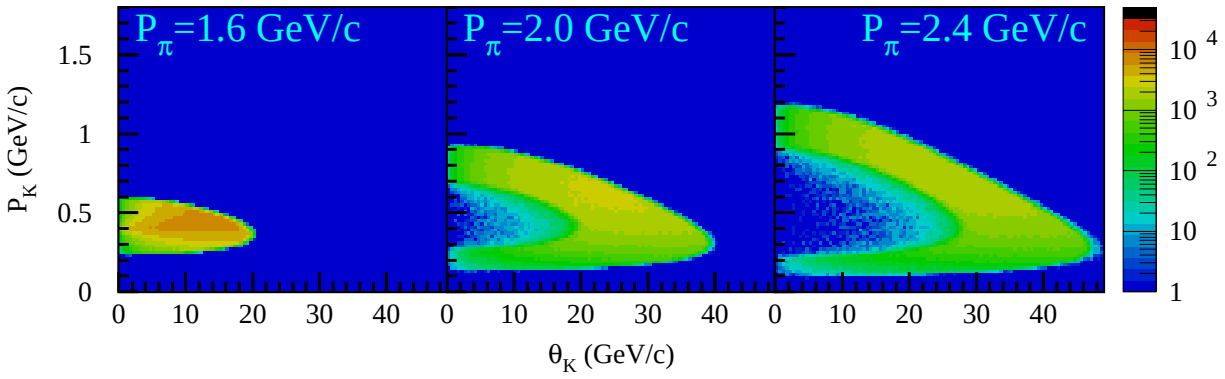

FIG. 19. Correlation between P_K and θ_K. At $P_\pi = 2.4$ GeV/c, the maximum θ_K is approximately 49°, and the maximum P_K is 1.19 GeV/c.

θ_K is approximately 49°. Fig. 18 shows the K momentum P_K as a function of θ_ϕ. The maximum P_K increases as increase of P_π. The maximum P_K is 1.19 GeV/c at P_π = 2.4 GeV/c. Figure 19 shows the correlation between P_K and θ_K.

What we have to do is to detect low-momentum charged kaons emitted at forward angles. It should be noted that the maximum P_K is 1.19 GeV/c and the maximum θ_K is 49.9° in the laboratory frame at $P_\pi \leq 2.4$ GeV/c.

III. EXPERIMENT

We measure the cross sections for the $\pi^- p \to \phi n$ reaction at incident pion momenta from 1.6 to 2.4 GeV/c using the modified E16 spectrometer with large acceptance for detecting K^+K^- pairs from the ϕ decays. Here, discussed are the negative-pion beam and the modified E16 spectrometer.

A. Negative-pion beam

Currently, the E16 experiment uses a 30-GeV primary proton beam at the high-momentum (high-p) beamline at J-PARC. The high-p beamline splits off from the main slow extraction beamline. The septum magnet (SM) for this split is located in the middle of the switchyard for slow extraction. A small fraction of the primary protons ($\approx 10^{10}$ Hz) are delivered at the high-p beamline. Since a production target can be placed at SM with 15-kW loss at maximum, high-intensity secondary pions can be produced and provided in principle at the beamline.

We have a lot of issues to be resolved for providing secondary particles at the high-p beamline fitted to the planned flagship experiment aiming at spectroscopy of charmed baryons [46]: a production target of secondary particles, polarity change of power supplies for magnets, kicker magnets, swinger magnets upstream and downstream of the production target, radiation shield, and regulations. It is necessary to develop production target which withstands heat from a 15-kW loss of the primary beam. Polarities of power supplies for magnets are currently fixed for the primary proton beam. Polarity-change of the power supplies are required for providing negatively-charged particles. To increase the intensity of secondary particles, collected should be emitted particles at forward angles. For this purpose,

we need to place swinger magnets upstream and downstream of the target. Additionally, we need a kicker magnet especially for the vertical direction to collect the secondary particles efficiently. Finally, we need additional radiation shield and new regulations.

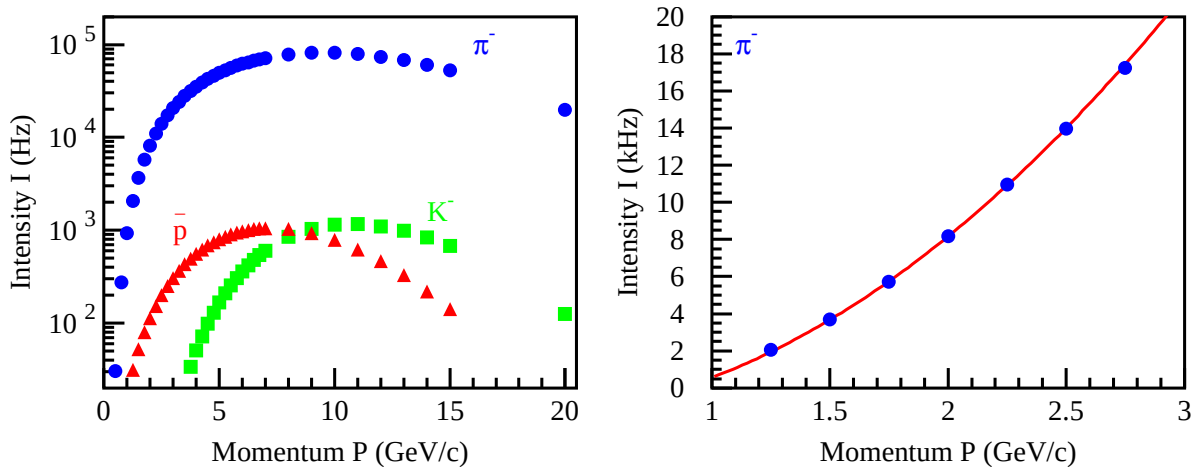

FIG. 20. Expected intensity of secondary negatively-charged particles as a function of the momentum for a 400-W loss of the primary proton beam. The left panel shows the intensities for π^- (blue), K^- (green), and $\bar{p}$ (red) at momenta below 20 GeV/c, and the right panel shows the π^- intensity at momenta ranging from 1 to 3 GeVc. The red curve represents the fitted quadratic function to the data shown in the right panel: $I/\mathrm{kHz} = 2.72\,\{P/\,(\mathrm{GeV}/c)\}^2 - 0.56P/\,(\mathrm{GeV}/c) - 1.61$.

Even though we do not place a dedicated production target, the collimator for the Lambertson magnet plays a role as a target for producing secondary particles. In this case, the expected intensity is 3.93, 5.40, 7.05, 8.87, 10.86 kHz at P_π = 1.6, 1.8, 2.0, 2.2, and 2.4 GeV/c, respectively, after optimizing the intensity with a 400-W loss of the primary proton beam without swinger magnets. Figure 20 shows the expected intensity of secondary negatively-charged particles as a function of the momentum. To provide a negative pion beam, the polarity change is required for power supplies for magnets. To increase the intensity, a kicker magnet for the vertical direction (V20) is also required. We may need to place additional radiation shield, and modify regulations slightly. We can hopefully use negative pions with a momentum of $\approx$ 2 GeV/c and an intensity of $\approx 10^4$ Hz at the 400-W loss, which is enough for studying ϕN resonances via the $\pi^- p \to \phi n$ reaction, just after the long shutdown period (2023–2025).

B. Modified E16 spectrometer

We plan to use the FM magnet for the E16 spectrometer as shown in Fig. 21. Each pole tip takes a cone shape, and the magnetic flux density in the central region is quite high ($\approx$ 1.8T). Figure 22 shows the magnetic flux density of the FM magnet along z, x, and y axes. Here, the z axis is taken along the central beam direction, and the y axis is defined as the vertical direction.

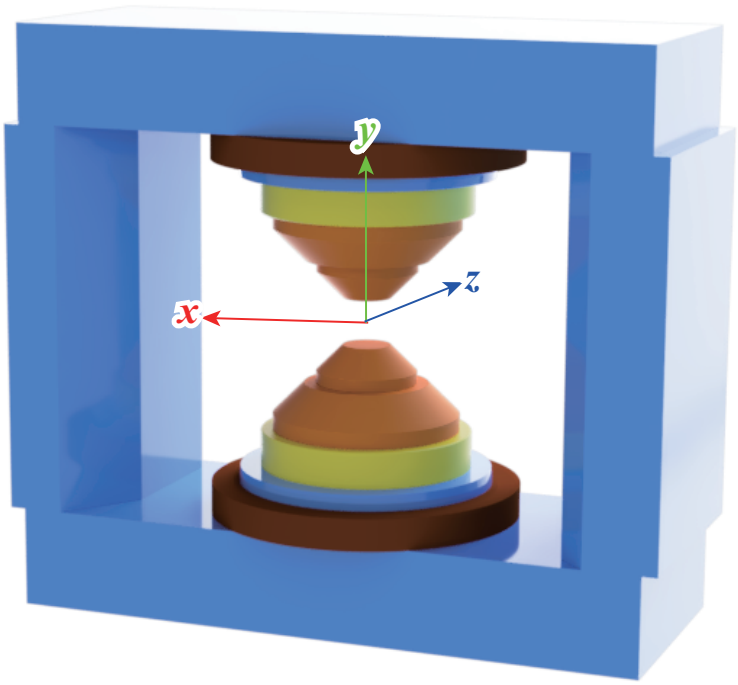

FIG. 21. Schematic view of the FM magnet and the definition of the axes. The z axis is taken along the central beam direction, and the y axis is defined as the vertical direction.

We use a part of the detector system for the E16 experiment. The E16 experiment aims at studying the medium modification of ϕ mesons by detecting e^+e^- pairs from the in-medium ϕ decays. The E16 detector system consists of tracking systems, and Cherenkov particle identification (PID) systems. The tracking system comprises a single layer of silicon strip detectors (SSDs), and three layers of gas electron multiplier (GEM) detectors, called the GEM trackers (GTRs), from the center. The PID system is comprised of hadron-blind detectors (HBDs) and lead-glass calorimeters (LGCs). The front faces of the LGCs are located at 1.4–1.6 m from the center. Both the HBDs and LGCs, covering the azimuthal

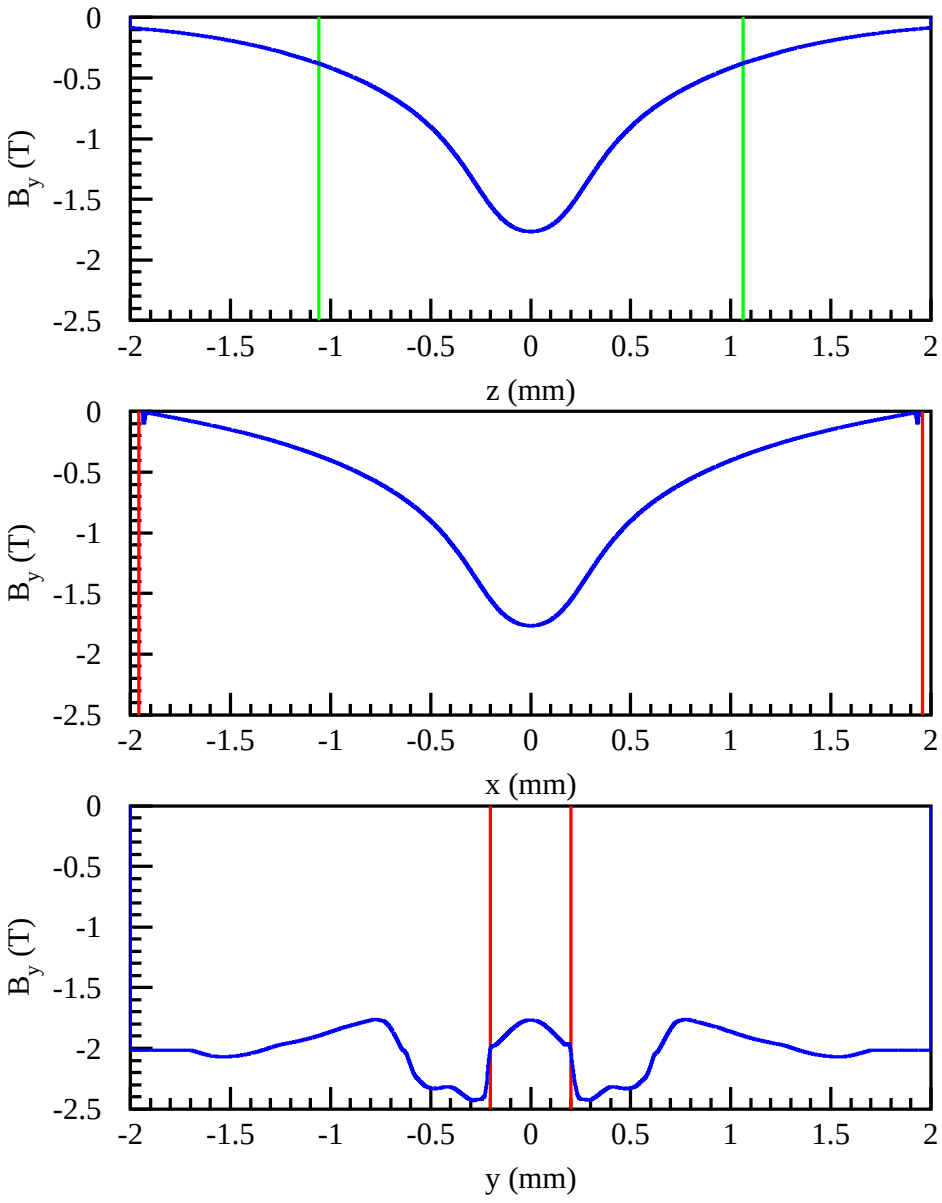

FIG. 22. Magnetic flux density of the FM magnet for the E16 spectrometer along z, x, and y axes. The green lines denote the entrance and exit surface of the yoke, and the red denote the boundaries of the yoke.

angles from 15° to 135° with respect to the central beam course on the horizontal plane, are used for identifying electrons and positrons. The GEM tracker covers the azimuthal angles from 15° to 112°. All the detectors cover the elevation and depression angles below 15° with respect to the horizontal plane. Figure. 23 shows the cross-sectional view of the E16 detector setup.

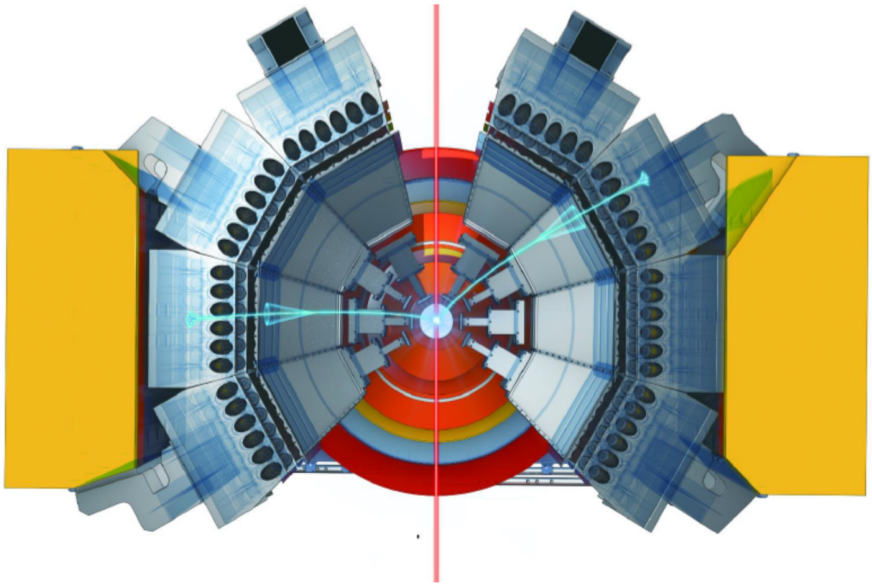

FIG. 23. Current E16 detector system. It covers the azimuthal angles from 15° to 135° (the tracking detectors cover only from 15° to 112°) with respect to the central beam course on the horizontal plane, and the elevation and depression angles below 15° with respect to the horizontal plane.

We detect rather slow charged kaons instead of electrons or positrons. Thus we do not use HBDs, and we use LGCs for measuring a stop timing for the time of light (TOF) for charged particle. We additionally place a hodoscope consisting of X-shaped acrylic Cherenkov detectors with a time resolution of approximately 45 ps for measuring a start timing for TOF, and place hodoscopes consisting of resistive plate chambers (RPCs) with a time resolution of approximately 65 ps just in front of LGCs to improve the time resolution for the TOF measurement. To enlarge the acceptance of detecting K^+K^- pairs from the ϕ decay, we additionally place tracking systems, and RPC hodoscopes or ordinary plastic-scintillator hodoscopes with a time resolution of approximately 60 ps at forward angles so that they cover the azimuthal angles less than 15° (corresponding height of $\pm$0.4 m) and the elevation and depression angles less than 30.9° (corresponding height of $\pm$0.9 m). Of course, we should cover more solid angles as long as possible. Here, we estimate the acceptance in the experimental setup described above.

C. Acceptance for detecting K^+K^- pairs

We estimate the acceptance of detecting K^+K^- pairs from the ϕ decay for a fixed P_π. We assume ϕs are generated isotropically in the CM frame, and each of them decays isotropically into a K^+K^- pair in the rest frame of the ϕ meson. Assumed to be detected are K^+s and K^-s coming to a cylindrical region within

1. $|\Psi_h| = 15°$–$112°$ and $|y| < 0.4$ m, or

2. $|\Psi_h| = 0°$–$15°$ and $|y| < 0.9$ m

at $\sqrt{x^2+y^2} = 1.5$ m, where $\Psi_h = \tan^{-1}(x/z)$. This angular coverage can be realized by combining the current E16 detector system and developing E50 detectors (PS hodoscopes and/or RPC hodoscopes). It should be noted that the maximum momentum of K mesons to be detected is 1.19 GeV/c, which makes the time difference of 0.38 ns between K and π for the 1.5-m travel. The TOF time resolution is high enough to separate K and π mesons even at the maximum momentum of 1.19 GeV/c since the measurements of start and stop timings are carried out with the time resolutions of $\approx$ 45 ps and $\approx$ 60 ps, repectively. Figure 24

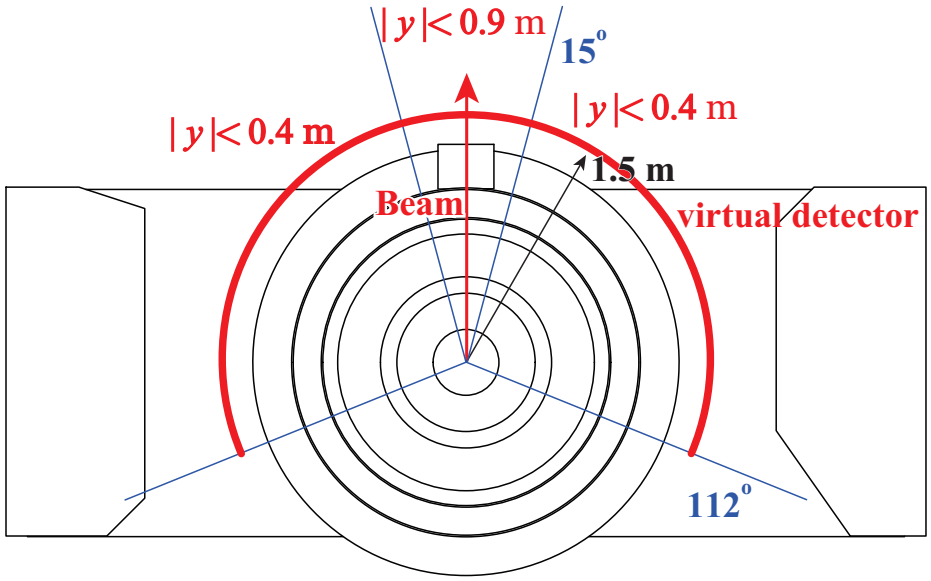

FIG. 24. Angular coverage of the detector system. We assume the detector system covers a cylindrical region within $|\Psi_h| = 15°$–$112°$ and $|y| < 0.4$ m or $|\Psi_h| = 0°$–$15°$ and $|y| < 0.9$ m at $\sqrt{x^2+y^2} = 1.5$ m.

shows the angular coverage of the detector system.

We estimate the geometrical acceptance, the probability that both K^+ and K^-, which do not decay in flight, arrive at a detector, and the acceptance including the effects of K^+ and K^- decays in flight. Table II summarizes the acceptances of detecting K^+K^- pairs from the ϕ decay for a fixed P_π. In this table, we show the acceptances for the minimum angular coverages at several incident pion momenta. Since the K^+s and K^-s from the ϕ decays are emitted at forward angles ($\theta_K < 49°$), we can get high geometrical acceptance only covering $|\Psi_h| < 45°$. Some of the K^+s and K^-s arrive at a detector with $|\Psi_h| \geq 45°$ owing to the magnetic flux density. To increase the geometrical acceptance, it is important to cover the $|\Psi_h| < 45°$ and the elevation and depression angles from $15°to45°$.

TABLE II. Acceptance of detecting K^+K^- pairs from the ϕ decay at a fixed P_π. The acceptance $\mathcal{A}_{\rm geo}$ denotes the probability that both K^+ and K^-, which do not decay in flight, arrive at the detector with a cylindrical region within $|\Psi_h| = 15°$–$112°$ and $|y| < 0.4$ m or $|\Psi_h| = 0°$–$15°$ and $|y| < 0.9$ m at $\sqrt{x^2+y^2} = 1.5$ m. Here, Ψ_h denotes $\tan^{-1}(x/z)$, and The acceptance $\mathcal{A}_{\rm det}$ includes the effects of K^+ and K^- decays in flight.

P_π	1.6 GeV/c	1.8 GeV/c	2.0 GeV/c	2.2 GeV/c	2.4 GeV/c
$\mathcal{A}_{\rm geo}$	0.636	0.460	0.448	0.456	0.469
$\mathcal{A}_{\rm det}$	0.234	0.207	0.227	0.249	0.272

We estimate the acceptance as a function of the ϕ-emission angle. Fig. 25 shows the acceptance of detecting K^+K^- pairs from the ϕ decay as a function of the ϕ-emission angle θ_ϕ for several P_πs. Geometrical acceptances for ϕ mesons emitted at backward angles ($\cos\theta_\phi < 0$) is lower, and they decrease with decrease of $\cos\theta_\phi$. The acceptance for detecting ϕ mesons is roughly a half of the geometrical one. To increase the acceptance for detecting ϕ mesons, it is important to shorten flight lengths from the vertex point of a $\phi \to K^+K^-$ decay to the detector for measuring the stop timing for TOF.

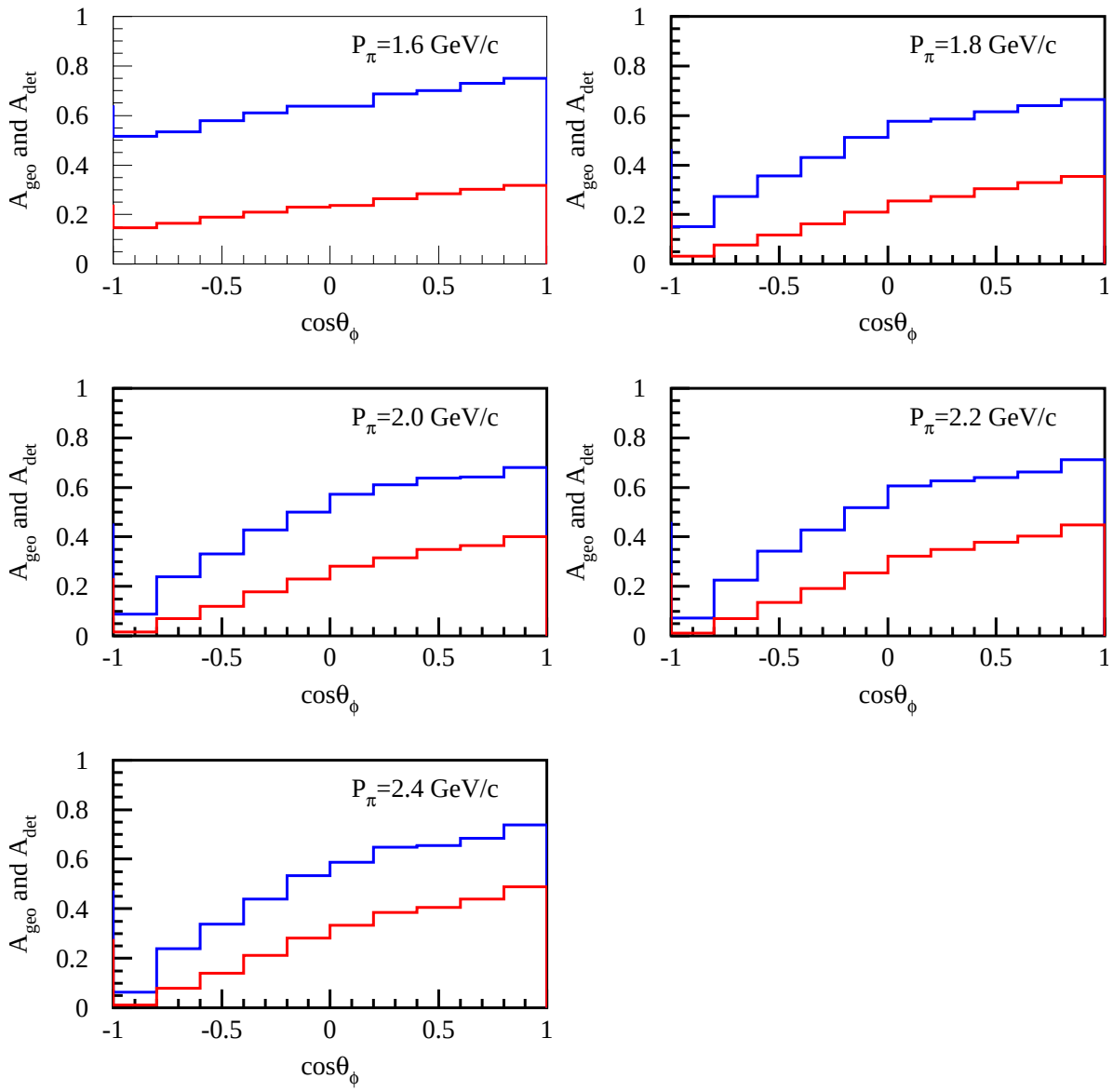

FIG. 25. Acceptance of detecting K^+K^- pairs from the ϕ decay as a function of the ϕ-emission angle θ_ϕ for several P_πs. The blue histograms show the geometrical acceptance $\mathcal{A}_{\rm geo}$ and the red the acceptance $\mathcal{A}_{\rm det}$ including the effects of K^+ and K^- decays in flight.

D. Yield estimation

We plan to use negative pion beams at incident momenta ranging from 1.6 to 2.4 GeV/c with a 0.2 GeV/c step. The total cross section assumed here is 20 μb. The target planned to be used is liquid deuterium with a thickness of 200 mm equivalent to approximately 0.90 b^{-1}. The branching ratio of the $\phi \to K^+K^-$ decay is 49.2% $\pm$ 0.5%. The secondary

beam extraction is made for the 2-s duration of every 5.2 s cycle, giving the duty factor is 0.385. If 10-kHz pions are provided as a beam, we obtain 2,900 $\phi \to K^+K^-$ events a day regardless of K^+K^- detection. The momentum bite is approximately $\pm 2\%$, corresponding to $\Delta W = 0.03$–0.04 GeV. The number of $\phi \to K^+K^-$ events for a W bin of 10 MeV in a day ranges from 740 to 980 depending on P_π. Since the acceptance for detecting K^+K^- pairs is 0.21–0.27 including the effects of K^+ and K^- decays in flight, 10-days measurement for each P_π gives approximately a few thousand events for each 10-MeV W bin. Table III summarizes the estimated number of the $\phi \to K^+K^-$ detection events for 10-days measurement and the W coverage.

TABLE III. Estimated number of the ϕ-produced events N_ϕ for 10-days measurement and the W coverage. Here, K^+ and K^- are detected without decaying in flight at 1.5-m downstream of the target center. The P_π, I_π, and $\mathcal{A}_{\rm det}$ denote the central incident pion momentum, the corresponding intensity of the pion beam for the 400-W loss, and the acceptance including the survival ratios of K^+ and K^-. The ΔW denotes the W coverage at a given P_π.

P_π	I_π	$\mathcal{A}_{\rm det}$	N_ϕ	ΔW
1.6 GeV/c	3.93 kHz	0.234	2710	30.20 MeV
1.8 GeV/c	5.40 kHz	0.207	3290	32.50 MeV
2.0 GeV/c	7.05 kHz	0.227	4710	34.70 MeV
2.2 GeV/c	8.87 kHz	0.249	6510	36.70 MeV
2.4 GeV/c	10.86 kHz	0.272	8700	38.70 MeV

Since the maximum intensity of the pion beam is ≈ 10 kHz, the hadron reaction rate is expected to be ≈ 0.36 kHz assuming the pion-nucleon total cross section of 40 mb. Thus, we can loose the trigger condition for data acquisition, which only requires two charged particle detection, or single $K^\pm$ detection, and so on. It should be noted that the dead time for processing an event in the data acquisition system for the E16 detector system is approximately 100 μs, which is limited by the readout from APV25 chips [50] used for tracking detectors.

IV. SUMMARY

Not clear is the origin of a resonance-like behavior at the CM energy of 2.2 GeV observed in the differential cross section $d\sigma/dt$ at $t = -|t|_{\rm min}$ as a function of the incident photon energy E_γ for ϕ photoproduction on the proton ($\gamma p \to \phi p$). The $d\sigma/dt$ at a fixed E_γ in $\gamma p \to \phi p$ shows a strong exponential behavior from the threshold, suggesting ϕ photoproduction is insensitive to s-channel ϕ-nucleon resonances. To reveal the origin of this bump, we would like to measure the angular differential cross section $d\sigma/d\Omega$ for pion-induced phi meson production on the proton ($\pi^- p \to \phi n$) at incident pion momenta ranging from 1.6 to 2.4 GeV/c. We plan to use secondary pions ($\approx$ 10 kHz) delivered at the high-p beamline with a 400-W loss of the primary proton beam at the Lambertson magnet. We utilize the E16 spectrometer magnet and the combined detector system of the E16 and E50 experiments, which provides high geometrical acceptance of detecting a K^+ and K^- pair from the ϕ decay. We expect to obtain a few thousand $\phi \to K^+K^-$ detection events at a fixed incident momentum covering the W width fro 0.03 to 0.04 GeV in 10-days measurement. We could confirm whether the same bump is observed in $\pi^- p \to \phi n$ or not from five sets of 10-days measurement (P_π = 1.6, 1.8, 2.0, 2.2, 2.4 GeV/c). Additionally, we need a 5-days beamtime for commissioning of the modified E16 detector system.

Appendix A: Exchange particle in $\pi^- p \to \phi n$ at high incident momenta

At high incident momenta, the dominant production mechanism of pion-induced ϕ production is t-channel exchange of some particle. Figure 26 shows the expected dominant diagram for $\pi^- p \to \phi n$. The negatively-charged pion (π^-) and ρ^- meson are candidates of the exchange particle for this reaction. Since the branching ratio of the $\phi \to \rho\pi$ decay ($\approx$ 15% including the $\phi \to \pi^+\pi^-\pi^0$ decay) is much larger than that of the $\phi \to \pi^+\pi^-$ decay ($\approx 10^{-4}$%) [24]. The ρ^- is considered to be a dominant contributor for exchange particles.

Nevertheless, the main contribution does not come from ρ^- exchange. Table IV summarizes some elements of the spin-density matrix in the helicity frame for $\pi^- p \to \phi n$. The elements of the spin density matrix ρ_{ij} of ϕ in $\pi^- p \to \phi n$ are described in the next section. Although the natural-parity exchange is expected owing to the nature of ρ, small is the sum of the two elements $\rho_{11} + \rho_{1-1}$ corresponding to the natural-parity exchange. Additionally,

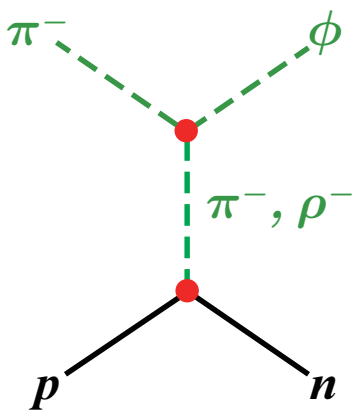

FIG. 26. Expected dominant diagram for $\pi^- p \to \phi n$ at high incident momenta. The π^- and ρ^- are candidates of the exchange particle.

a sizable ρ_{00} and a large $\rho_{11} - \rho_{1-1}$ suggest the large contribution of the unnatural-parity exchange. There is a possibility that the elements indicating unnatural-parity exchange come from the effects of s-channel and that more ρ exchange takes place at higher incident momenta since $\rho_{11} + \rho_{1-1}$ increases and $\rho_{11} - \rho_{1-1}$ decreases with increase of incident pion momentum. Or other particle such as $b_1(1235)$ possibly having the $s\bar{s}$ component could play a dominant role in t-channel exchange since neither π nor ρ has $s\bar{s}$ component.

TABLE IV. Elements of the spin-density matrix of ϕ in the helicity frame for $\pi^- p \to \phi n$ taken from Ref. [43].

P_π	$-t'$	$\rho_{11} + \rho_{1-1}$	ρ_{00}	$\rho_{11} - \rho_{1-1}$	Re[ρ_{10}]
4 GeV/c	0.15–0.90 GeV$^2/c^2$	0.12 ± 0.14	0.26 ± 0.17	0.61 ± 0.17	0.14 ± 0.10
5 and 6 GeV/c (average)	0.15–0.90 GeV$^2/c^2$	0.38 ± 0.08	0.20 ± 0.09	0.43 ± 0.09	0.06 ± 0.05

Appendix B: Spin density matrix of ϕ in $\pi^- p \to \phi n$

Ref. [48] provides the formalism to analyze vector meson production with polarized photons in detail. Here, spin density matrix (SDM) of ϕ is given for $\pi^- p \to \phi n$. The π is a spinless particle giving only one SDM element $\rho_{00} = 1$. The polarization state of ϕ is expressed in terms of its spin space density matrix $\rho(\phi)$, which is connected by the production

amplitudes T:

$$\rho(\phi) = T\rho(\pi)T^{\dagger}. \tag{B1}$$

In the helicity frame, SDM of ϕ is described in the following equation:

$$\rho_{\lambda_\phi\lambda'_\phi}(\phi) = \frac{1}{N}\sum_{\lambda_n\lambda_p} T_{\lambda_\phi\lambda_n,0\lambda_p}\rho_{00}(\pi)T^{*}_{\lambda'_\phi\lambda_n,0\lambda_p} \tag{B2}$$

where λs denotes the helicities of the respective particles of the $\pi^- p \to \phi n$ reaction, and N is the normalization factor:

$$N = \frac{1}{2}\sum_{\lambda_\phi,\lambda_n,\lambda_p} \left|T_{\lambda_\phi\lambda_n,0\lambda_p}\right|^2. \tag{B3}$$

The normalization of T is chosen so that the production cross section is given by

$$\frac{d\sigma}{d\Omega} = \left(\frac{2\pi}{k}\right)^2 \frac{1}{2}\sum_{\lambda_\phi,\lambda_n,\lambda_p} \left|T_{\lambda_\phi\lambda_n,0\lambda_p}\right|^2 \tag{B4}$$

where k denotes the incident pion momentum.

We consider the $\phi \to K^+K^-$ decay where a vector meson decays into two spinless particles. The decay angular distribution of Ks from the ϕ-decay is discussed in the helicity of ϕ. The z direction is chosen opposite to the direction of the outgoing neutron n in the rest system of ϕ. The y direction is the normal to the production plane, defined by the cross product $\hat{k}\times\hat{q}$ of the three-momenta $\hat{k}$ of the incident π and that $\hat{q}$ of the produced ϕ. The x direction is given by $\hat{x} = \hat{y}\times\hat{z}$. The decay angles θ and ϕ of K corresponding to the momentum direction $\hat{\pi}$ are defined as the polar and azimuthal angles of Ks in the rest frame of ϕ. The θ and ϕ for giving the decay angles satisfy

$$\begin{aligned} \cos\theta &= \hat{\pi}\cdot\hat{z}, \\ \cos\phi &= -\frac{\hat{y}\cdot(\hat{z}\times\hat{\pi})}{|\hat{z}\times\hat{\pi}|}, \text{ and} \\ \sin\phi &= -\frac{\hat{x}\cdot(\hat{z}\times\hat{\pi})}{|\hat{z}\times\hat{\pi}|}. \end{aligned} \tag{B5}$$

The decay angular distribution of K in the rest frame of ϕ reads:

$$W(\theta,\phi) \equiv \frac{dN}{d\cos\theta\, d\phi} = \sum_{\lambda_\phi,\lambda'_\phi} \langle\theta,\phi\,|M\,|\lambda_\phi\,\rangle\,\rho_{\lambda_\phi,\lambda'_\phi}\,\langle\lambda'_\phi\,|M^*\,|\theta,\phi\,\rangle \tag{B6}$$

where M is the decay amplitude:

$$\langle\theta,\phi\,|M\,|\lambda_\phi\,\rangle = C\sqrt{\frac{3}{4\pi}}D^{1*}_{\lambda_\phi 0}\,(\phi,\theta,-\phi)\,. \tag{B7}$$

The quantity $|C|^2$ is proportional to the decay width of ϕ. We consider a normalized decay angular distribution, we chose $C = 1$. The Wigner rotation function D is given by

$$\begin{aligned} D^1_{10}\left(\phi,\theta,-\phi\right) &= -\frac{1}{\sqrt{2}}\sin\theta\exp\left(-i\phi\right), \\ D^1_{00}\left(\phi,\theta,-\phi\right) &= \cos\theta, \text{ and} \\ D^1_{-10}\left(\phi,\theta,-\phi\right) &= +\frac{1}{\sqrt{2}}\sin\theta\exp\left(+i\phi\right). \end{aligned} \tag{B8}$$

The decay angular distribution (B6) can be written as

$$W(\theta,\phi) = \frac{3}{4\pi}\sum_{\lambda_\phi,\lambda'_\phi} D^{1*}_{\lambda_\phi 0}\left(\phi,\theta,-\phi\right)\rho(\phi)_{\lambda_\phi,\lambda'_\phi} D^1_{\lambda'_\phi 0}\left(\phi,\theta,-\phi\right). \tag{B9}$$

Using the fact that the $\rho(\phi)$ is hermitian, $\rho(\phi)_{\lambda_\phi,\lambda'_\phi} = \rho^*(\phi)_{\lambda'_\phi,\lambda_\phi}$, we obtain

$$\begin{aligned} W(\theta,\phi) = \frac{3}{4\pi}\Big\{ & \frac{1}{2}\left(\rho_{11}+\rho_{-1-1}\right)\sin^2\theta + \rho_{00}\cos^2\theta \\ & + \frac{1}{\sqrt{2}}\left(-\mathrm{Re}[\rho_{10}] + \mathrm{Re}[\rho_{-10}]\right)\sin 2\theta\cos\phi \\ & + \frac{1}{\sqrt{2}}\left(\mathrm{Im}[\rho_{10}] + \mathrm{Im}[\rho_{-10}]\right)\sin 2\theta\sin\phi \\ & - \mathrm{Re}[\rho_{1-1}]\sin^2\theta\cos 2\phi + \mathrm{Im}[\rho_{1-1}]\sin^2\theta\cos 2\phi\Big\} \end{aligned} \tag{B10}$$

Now, let's discuss separation of natural- and unnatural-parity exchange contributions using the symmetry properties of the helicity amplitudes:

$$T_{-\lambda_\phi-\lambda_n,-\lambda_\pi-\lambda_p} = (-1)^{\left(\lambda_\phi-\lambda_n\right)-\left(\lambda_\pi-\lambda_p\right)} T_{\lambda_\phi\lambda_n,\lambda_\pi\lambda_p}, \tag{B11}$$

where $\lambda_\pi = 0$ because π^- is a spinless particle. Considering pure t-channel exchange of a particle with a spin-parity of J^π,

$$T_{-\lambda_\phi\lambda_n,-\lambda_\pi\lambda_p} = \pi\pi_\phi\pi_\pi(-1)^{J+J_\phi-J_\pi+\lambda_\phi-\lambda_\pi} T_{\lambda_\phi\lambda_n,\lambda_\pi\lambda_p}. \tag{B12}$$

Hence, the production amplitude for the natural-parity exchange reads:

$$T^N_{-\lambda_\phi\lambda_n,0\lambda_p} = -(-1)^{\lambda_\phi} T^N_{\lambda_\phi\lambda_n,0\lambda_p}, \text{ and} \tag{B13}$$

that for the unnatural-parity exchange reads:

$$T^U_{-\lambda_\phi\lambda_n,0\lambda_p} = +(-1)^{\lambda_\phi} T^U_{\lambda_\phi\lambda_n,0\lambda_p}. \tag{B14}$$

From Eqs. (B13) and (B14), the following projection relations are obtained:

$$\begin{aligned} T^N_{\lambda_\phi\lambda_n,0\lambda_p} &= \frac{1}{2}\left(T_{\lambda_\phi\lambda_n,0\lambda_p} - (-1)^{\lambda_\phi} T_{-\lambda_\phi\lambda_n,0\lambda_p}\right), \text{ and} \\ T^U_{\lambda_\phi\lambda_n,0\lambda_p} &= \frac{1}{2}\left(T_{\lambda_\phi\lambda_n,0\lambda_p} + (-1)^{\lambda_\phi} T_{-\lambda_\phi\lambda_n,0\lambda_p}\right). \end{aligned} \tag{B15}$$

Thus, the parity conservation reduces the number of independent matrix elements

$$\rho_{\lambda\lambda'} = (-1)^{\lambda-\lambda'}\rho_{-\lambda-\lambda'}. \tag{B16}$$

Using $\rho_{-1-1} = \rho_{11}$ and $\mathrm{Im}[\rho_{1-1}] = 0$, the decay angular distribution (B10) reads:

$$\begin{aligned} W(\theta,\phi) = \frac{3}{4\pi}\Big\{ & \rho_{00}\cos^2\theta + (\rho_{11}-\rho_{1-1})\sin^2\theta\cos^2\phi \text{ [unnatural-parity exchange]} \\ & + (\rho_{11}+\rho_{1-1})\sin^2\theta\sin^2\phi \text{ [natural-parity exchange]} \\ & - \sqrt{2}\mathrm{Re}[\rho_{10}]\sin 2\theta\cos\phi\Big\}. \end{aligned} \tag{B17}$$

The $\rho_{11} + \rho_{1-1}$ corresponds to the natural-parity exchange contribution, and the ρ_{00} and $\rho_{11} - \rho_{1-1}$ provide the unnatural-parity exchange.

Appendix C: Study of P_c baryons via $\pi^- p \to J/\psi n$

Recently, the LHCb collaboration observed exotic hidden-charm P_c baryons in the $J/\psi p$ invariant-mass distributions for the $\Lambda_b \to J/\psi p K^-$ decay [6, 7]. However, corresponding peaks are not observed in the total cross section measured by the GlueX collaboration as a function of the incident photon energy for J/ψ photoproduction on the proton ($\gamma p \to J/\psi p$) [11]. Similarly to $\gamma p \to \phi p$, $\gamma p \to J/\psi p$ is insensitive to s-channel $J/\psi p$ resonances. It is very important to confirm these P_c baryons in other possible reactions such as $\pi^- p \to J/\psi n$ which is expected to be much more sensitive to s-channel $J/\psi p$ resonances. In Ref. [21], the total cross section predicted is 1 nb near the P_c masses for $\pi^- p \to J/\psi n$, while that for the background processes is the order of 10^{-4}–10^{-3} nb. In Ref. [47], the total cross section is 1 μb . Although it is much larger than that in Ref. [21], it is still small to produce J/ψs with $\approx$ 100-kHz pion beams. When we get higher intensity pion beam and a dedicated system for detecting J/ψ, we should measure the cross sections for $\pi^- p \to J/\psi n$.

Appendix D: Study of ϕN interaction via the near-threshold $\pi^- p \to \phi n$ reaction

Because the ϕ meson is unstable and neutral, it is difficult to obtain a ϕ-meson beam for scattering experiments. However, by analyzing the total cross section near the threshold, the scattering length can be estimated. Here, two methods are briefly introduced to determine the scattering length.

The first one is the determination of the imaginary part of the scattering length by fitting a linear function to the total cross section as a function of the relative momentum in the final state. This method is applied for determining the lower limit of the imaginary part of the ηN scattering length in the $\pi^- p \to \eta n$ reaction [49]. The optical theorem leads to the equation:

$$\begin{aligned}
\mathrm{Im}[a_{\eta N}] &= \frac{p_\eta}{4\pi}\sigma_{\eta n} \\
&= \frac{p_\eta}{4\pi}\left(\sigma_{\eta n\to\pi N} + \sigma_{\eta n\to\pi\pi N} + \sigma_{\eta n\to\eta N}\right) \\
&= \frac{3p_\pi^2}{8\pi p_\eta}\sigma_{\pi^- p\to\eta n} + \frac{p_\eta}{4\pi}\left(\sigma_{\eta n\to\pi\pi N} + \sigma_{\eta n\to\eta N}\right), \\
&\geq \frac{3p_\pi^2}{8\pi p_\eta}\sigma_{\pi^- p\to\eta n}
\end{aligned} \tag{D1}$$

where p_π and p_η denotes the relative momentum in the πN and ηN CM frame, respectively. The fitting result of $\sigma_{\pi^- p\to\eta n}/p_\eta = 15.2 \pm 0.8$ μb/MeV gives $\mathrm{Im}[a_{\eta N}] \geq 0.172 \pm 0.009$ fm. Similarly, we can determine the lower limit of $\mathrm{Im}[a_{\phi N}]$.

In Ref. [36], we have determined the complex scattering length $a_{\omega p}$ and effective range $r_{\omega p}$ from the shape of the total cross section as a function of E_γ (excitation function) for $\gamma p \to \omega p$. Here, we evaluate the excitation function for the $\gamma p \to \omega p$ reaction using a model with final-state ωp interaction (FSI) based on the Lippmann-Schwinger equation. We assume that the S-wave contribution is dominant near the threshold. The total cross section for a fixed ω mass M and γp-CM energy W can be calculated using a transition amplitude $T_{\gamma p\to\omega p}(W, M)$:

$$\sigma_0(W, M) = \frac{1}{16\pi W^2}\frac{p(W, M)}{k}\left|T_{\gamma p\to\omega p}(W, M)\right|^2, \tag{D2}$$

where k and p denote the momenta of an initial- and a final-state particles, respectively, in the γp-CM frame. The total cross section σ as a function of E_γ is obtained by averaging $\sigma_0(W(E_\gamma), M)$ over available ω masses:

$$\sigma(E_\gamma) = \int_{m_{\pi^0}}^{W(E_\gamma)-m_p} \sigma_0(W(E_\gamma), M) L_\omega(M) dM, \tag{D3}$$

where the probability $L_\omega(M)$ stands for a Breit-Wigner function with a centroid of $M_\omega = 782.65$ MeV and a width of $\Gamma_\omega = 8.49$ MeV [24]. Since ω is identified with the $\pi^0\gamma$ decay mode in Ref. [36], the lower limit of the running ω mass is the π^0 mass.

The $T_{\gamma p\to\omega p}$ is expressed by

$$T_{\gamma p\to\omega p} = V_{\gamma p\to\omega p} + T_{\omega p\to\omega p} G_{\omega p\to\omega p} V_{\gamma p\to\omega p}, \tag{D4}$$

where $T_{\omega p\to\omega p}$ denotes the ωp scattering amplitude, $G_{\omega p\to\omega p}$ denotes the ωp propagator, and $V_{\gamma p\to\omega p}$ is the production amplitude without FSI. We obtain the matrix element for $T_{\gamma p\to\omega p}$ with on-shell approximations for $T_{\omega p\to\omega p}$ and $V_{\gamma p\to\omega p}$, and introduce a Gaussian form factor in the integration of $G_{\omega p\to\omega p}$. This leads the matrix element of $T_{\gamma p\to\omega p}$ to the equation:

$$\begin{aligned}
&\left\langle \omega p(p) \left| T_{\gamma p\to\omega p} \right| \gamma p(k) \right\rangle \\
&\quad = \left\langle \omega p(p) \left| V_{\gamma p\to\omega p} \right| \gamma p(k) \right\rangle \\
&\qquad + \int \left\langle \omega p(p) \left| T_{\omega p\to\omega p} \right| \omega p(q) \right\rangle \frac{\delta^3(\vec{q}-\vec{q}\,')}{W - H_0 + i\epsilon} \left\langle \omega p(q') \left| V_{\gamma p\to\omega p} \right| \gamma p(k) \right\rangle d\vec{q}\, d\vec{q}\,' \\
&\quad \simeq \left[1 + 8\pi\mu \left\langle \omega p(p) \left| T_{\omega p\to\omega p} \right| \omega p(p) \right\rangle \int \frac{d\vec{q}}{p^2 - q^2 + i\mu\Gamma_\omega} \exp\left(-\frac{q^2}{\Lambda^2}\right) \right] \\
&\qquad \left\langle \omega p(p) \left| V_{\gamma p\to\omega p} \right| \gamma p(k) \right\rangle,
\end{aligned} \tag{D5}$$

where H_0 denotes the free Hamiltonian for the final-state ωp, μ is a reduced mass between ω with a mass of M and the proton, and a cut-off parameter Λ. The $\left\langle \omega p(p) \left| T_{\omega p\to\omega p} \right| \omega p(p) \right\rangle$ is given by $a_{\omega p}$ and $r_{\omega p}$:

$$\left\langle \omega p(p) \left| T_{\omega p\to\omega p} \right| \omega p(p) \right\rangle = -\frac{1}{(2\pi)^2 \mu} \left(\frac{1}{a_{\omega p}} + \frac{1}{2} r_{\omega p} p^2 - ip \right)^{-1}. \tag{D6}$$

The $\left\langle \omega p(p) \left| V_{\gamma p\to\omega p} \right| \gamma p(k) \right\rangle$ is assumed to be a constant value of 1 in the incident-energy region of interest. The 1/2 and 3/2 spin-averaged scattering length $a_{\omega p}$ and effective range $r_{\omega p}$ between the ω meson and proton are determined from the shape of the total cross section as a function of the incident photon energy: $a_{\omega p} = \left(-0.97^{+0.16_{\rm stat}\,+0.03_{\rm syst}}_{-0.16_{\rm stat}\,-0.00_{\rm syst}}\right) + i\left(0.07^{+0.15_{\rm stat}\,+0.17_{\rm syst}}_{-0.14_{\rm stat}\,-0.09_{\rm syst}}\right)$ fm and $r_{\omega p} = \left(+2.78^{+0.67_{\rm stat}\,+0.11_{\rm syst}}_{-0.54_{\rm stat}\,-0.12_{\rm syst}}\right) + i\left(-0.01^{+0.46_{\rm stat}\,+0.06_{\rm syst}}_{-0.50_{\rm stat}\,-0.00_{\rm syst}}\right)$ fm.

Similarly to the determination of the low-energy ωp scattering parameters, we can deduce the low-energy ϕN scattering parameters from the total cross section as a function of the incident pion momentum for $\pi^- p \to \phi n$. For this purpose, we need a precise measurement

of the total cross sections with fine binning near the threshold.

---

[1] F. E. Close, *"An Introduction to Quarks and Partons,"* Academic Press, 1979.

[2] A. Hosaka and H. Toki, *"Quarks, baryons and chiral symmetry,"* World Scientific, 2001.

[3] M. Oka and K. Yazaki, *"Short Range Part of Baryon Baryon Interaction in a Quark Model. 1. Formulation,"* Prog. Theor. Phys. **66**, 556–571 (1981).

[4] M. Oka and K. Yazaki, *"Short Range Part of Baryon Baryon Interaction in a Quark Model. 2. Numerical Results for S-Wave,"* Prog. Theor. Phys. **66**, 572–587 (1981).

[5] V. D. Burkert, *"N^* Experiments and what they tell us about Strong QCD Physics,"* EPJ Web Conf. **241**, 01004 (2020).

[6] R. Aaij *et al.* (LHCb collaboration), *"Observation of $J/\psi p$ Resonances Consistent with Pentaquark States in $\Lambda_b^0 \to J/\psi K^- p$ Decays,"* Phys. Rev. Lett. **115**, 072001 (2015).

[7] R. Aaij *et al.* (LHCb collaboration), *"Observation of a narrow pentaquark state, $P_c(4312)^+$, and of two-peak structure of the $P_c(4450)^+$,"* Phys. Rev. Lett. **122**, 222001 (2019).

[8] T. Mibe *et al.* (LEPS collaboration), *"Diffractive phi-meson photoproduction on proton near threshold,"* Phys. Rev. Lett. **95**, 182001 (2005).

[9] B. Dey *et al.* (CLAS collaboration), *"Data analysis techniques, differential cross sections, and spin density matrix elements for the reaction $\gamma p \to \phi p$,"* Phys. Rev. C **89**, 055208 (2014).

[10] K. Mizutani *et al.* (LEPS collaboration), *"ϕ photoproduction on the proton at E_γ = 1.5–2.9 GeV,"* Phys. Rev. C **96**, 062201 (2017).

[11] A. Ali *et al.* (GlueX collaboration), *"First Measurement of Near-Threshold J/ψ Exclusive Photoproduction off the Proton,"* Phys. Rev. Lett. **123**, 072001 (2019).

[12] I. I. Strakovsky, L. Pentchev and A. I. Titov, *"Comparative analysis of ωp, ϕp, and $J/\psi p$ scattering lengths from A2, CLAS, and GlueX threshold measurements,"* Phys. Rev. C **101**, 045201 (2020).

[13] S. Acharya *et al.* (ALICE collaboration), *"Experimental Evidence for an Attractive p-ϕ Interaction,"* Phys. Rev. Lett. **127**, 172301 (2021).

[14] Y. Lyu, T. Doi, T. Hatsuda, Y. Ikeda, J. Meng, K. Sasaki and T. Sugiura, *"Attractive N-ϕ Interaction and Two-Pion Tail from Lattice QCD near Physical Point,"* arXiv: 2205.10544 [hep-lat].

[15] A. Kiswandhi, J. J. Xie and S. N. Yang, *"Is the nonmonotonic behavior in the cross section of phi photoproduction near threshold a signature of a resonance?,"* Phys. Lett. B **691**, 214–218 (2010).

[16] H. Seraydaryan *et al.* (CLAS collaboration), *"ϕ-meson photoproduction on Hydrogen in the neutral decay mode,"* Phys. Rev. C **89**, 055206 (2014).

[17] S. Y. Ryu *et al.* (LEPS collaboration), *"Interference effect between ϕ and $\Lambda(1520)$ production channels in the $\gamma p \to K^+K^-p$ reaction near threshold,"* Phys. Rev. Lett. **116**, 232001 (2016).

[18] H. Y. Ryu, A. I. Titov, A. Hosaka and H. C. Kim, *"ϕ photoprodution with coupled-channel effects,"* Prog. Theor. Exp. Phys. **2014**, 023D03 (2014).

[19] A. I. Titov and T. S. H. Lee, *"Spin effects and baryon resonance dynamics in phi meson photoproduction at few GeV,"* Phys. Rev. C **67**, 065205 (2003).

[20] T. Nakano and H. Toki, *"Glueball hunt in Phi photoproduction,"* in proceedings of the 5th Tamura Symposium: International Workshop on Exciting Physics with New Accelerators Facilities (EXPAF 97), 48–54 (1997).

[21] S. H. Kim, H. C. Kim and A. Hosaka, *"Heavy pentaquark states $P_c(4380)$ and $P_c(4450)$ in the J/ψ production induced by pion beams off the nucleon,"* Phys. Lett. B **763**, 358–364 (2016).

[22] E. Oset and A. Ramos, *"Dynamically generated resonances from the vector octet-baryon octet interaction,"* Eur. Phys. J. A **44**, 445–454 (2010).

[23] A. Ramos and E. Oset, *"The role of vector-baryon channels and resonances in the $\gamma p \to K^0\Sigma^+$ and $\gamma n \to K^0\Sigma^0$ reactions near the $K^*\Lambda$ threshold,"* Phys. Lett. B **727**, 287–292 (2013).

[24] P. A. Zyla *et al.* [Particle Data Group], *"Review of Particle Physics,"* PTEP **2020**, 083C01 (2020).

[25] H. X. Chen, W. Chen, X. Liu and S. L. Zhu, *"The hidden-charm pentaquark and tetraquark states,"* Phys. Rept. **639**, 1–121 (2016).

[26] A. Esposito, A. Pilloni and A. D. Polosa, *"Multiquark Resonances,"* Phys. Rept. **668**, 1–97 (2017).

[27] A. Ali, J. S. Lange and S. Stone, *"Exotics: Heavy Pentaquarks and Tetraquarks,"* Prog. Part. Nucl. Phys. **97**, 123–198 (2017).

[28] M. L. Du, V. Baru, F. K. Guo, C. Hanhart, U. G. Meißner, A. Nefediev and I. Strakovsky, *"Deciphering the mechanism of near-threshold J/ψ photoproduction,"* Eur. Phys. J. C **80**, 1053 (2020).

[29] Y. Koike and A. Hayashigaki, *"QCD sum rules for rho, omega, phi meson - nucleon scattering lengths and the mass shifts in nuclear medium,"* Prog. Theor. Phys. **98**, 631–652 (1997).

[30] A. I. Titov, T. Nakano, S. Date and Y. Ohashi, *"Comments on differential cross-section of phi-meson photoproduction at threshold,"* Phys. Rev. C **76**, 048202 (2007).

[31] W. C. Chang *et al. "Forward coherent phi-meson photoproduction from deuterons near threshold,"* Phys. Lett. B **658**, 209–215 (2008).

[32] T. Ishikawa *et al. "ϕ photo-production from Li, C, Al, and Cu nuclei at $E_\gamma = 1.5$–2.4 GeV,"* Phys. Lett. B **608**, 215–222 (2005).

[33] R. Lednický and V. L. Lyuboshits, *"Final State Interaction Effect on Pairing Correlations Between Particles with Small Relative Momenta,"* Yad. Fiz. **35**, 1316–1330 (1981).

[34] E. L. Feinberg, *"Hadron Clusters and Half Dressed Particles in Quantum Field Theory,"* Sov. Phys. Usp. **23**, 629–650 (1980).

[35] Y. Z. Xu, S. Chen, Z. Q. Yao, D. Binosi, Z. F. Cui and C. D. Roberts, *"Vector-meson production and vector meson domina nce,"* Eur. Phys. J. C **81**, 895 (2021).

[36] T. Ishikawa *et al. "ωN scattering length from ω photoproduction on the proton near the threshold,"* Phys. Rev. C **101**, 052201 (2020).

[37] R. Muto *et al.* [KEK-PS-E325], *"Evidence for in-medium modification of the phi meson at normal nuclear density,"* Phys. Rev. Lett. **98**, 042501 (2007).

[38] S. Yokkaichi, H. En'yo, M. Naruki, R. Muto, T. Tabaru, K. Ozawa, H. Hamagaki, K. Shigaki, S. Sawada, M. Sekimoto *et al.*, "Electron pair spectrometer at the J-PARC 50-GeV PS to explore the chiral symmetry in QCD," Proposals for Nuclear and Particle Physics Experiments at J-PARC, KEK/J-PARC-PAC 2006-06 (2006).

[39] O. I. Dahl, L. M. Hardy, R. I. Hess, J. Kirz and D. H. Miller, *"Strange-particle production in π^- p interactions from 1.5 to 4.2 BeV/c. 1. Three-and-more-body final states,"* Phys. Rev. **163**, 1377–1429 (1967).

[40] J. H. Boyd, A. R. Erwin, W. D. Walker, and E. West, *"Study of $\pi^- p \to \omega n, \phi n$ at 2.10 BeV/c,"* Phys. Rev. **166**, 1458–1472 (1968).

[41] D. Bollini, A. Buhler-Broglin, P. Dalpiaz, T. Massam, F. Navach, F. L. Navarria, M. A. Schneegans and A. Zichichi, *"A measurement of the ϕ-meson production cross-section in $\pi^- p$ interactions at 2.13 GeV/c,"* Il Nuovo Cimento A **60**, 541–554 (1969).

[42] B. D. Hyams, W. Koch, D. C. Potter, L. Von Lindern, E. Lorenz, G. Luetjens, U. Stierlin and

P. Weilhammer, *"The reaction $\pi^- p \to K^+ K^- n$ between 988 and 1100 MeV invariant KK mass,"* Nucl. Phys. B **22**, 189–204 (1970).

[43] D. S. Ayres, R. Diebold, A. F. Greene, S. L. Kramer, J. S. Levine, A. J. Pawlicki and A. B. Wicklund, *"ϕ Meson Production in $\pi^- p$ and $K^- p$ Interactions from 3-GeV/c to 6-GeV/c,"* Phys. Rev. Lett. **32**, 1463 (1974).

[44] H. Courant, Y. I. Makdisi, M. L. Marshak, E. A. Peterson, K. Ruddick and J. Smith-Kintner, *"ϕ Production in $\pi^- p$ Collisions Near Threshold,'* Phys. Rev. D **16**, 1-6 (1977).

[45] S. V. Golovkin *et al. "Study of the OZI selection rule in hadronic processes,"* Z. Phys. A **359**, 435–444 (1997).

[46] H. Noumi, Y. Morino, T. Nakano, K. Shirotori, Y. Sugaya, T. Yamaga, K. Ozawa, T. Ishikawa, Y. Miyachi and K. Tanida, *"Charmed Baryon Spectroscopy via the (π^-, D^{*-}) reaction,"* Proposals for Nuclear and Particle Physics Experiments at J-PARC, KEK/J-PARC-PAC 2012-19 (2013).

[47] Q. F. Lü, X. Y. Wang, J. J. Xie, X. R. Chen and Y. B. Dong, *"Neutral hidden charm pentaquark states $P_c^0(4380)$ and $P_c^0(4450)$ in $\pi^- p \to J/\psi n$ reaction,"* Phys. Rev. D **93**, 034009 (2016).

[48] K. Schilling, P. Seyboth and G. E. Wolf, *"On the Analysis of Vector Meson Production by Polarized Photons,"* Nucl. Phys. B **15**, 397–412 (1970).

[49] R. A. Arndt, W. J. Briscoe, I. I. Strakovsky and R. L. Workman, *"Extended partial-wave analysis of πN scattering data,"* Phys. Rev. C **74**, 045205 (2006).

[50] L. L. Jones, M. J. French, Q. Morrissey, A. Neviani, M. Raymond, G. Hall, P. Moreira and G. Cervelli, *"The APV25 deep submicron readout chip for CMS detectors,"* Conf. Proc. C **9909201**, 162–166 (1999).